

# Enhanced stability of free viscous films due to surface viscosity

Cite as: Phys. Fluids **32**, 082108 (2020); <https://doi.org/10.1063/5.0016282>

Submitted: 03 June 2020 . Accepted: 22 July 2020 . Published Online: 13 August 2020

Anjishnu Choudhury, Venkatesh Kumar Paidi , Sreeram K. Kalpathy , and Harish N. Dixit 



View Online



Export Citation



CrossMark

## ARTICLES YOU MAY BE INTERESTED IN

[Inertial migration of spherical particles in channel flow of power law fluids](#)

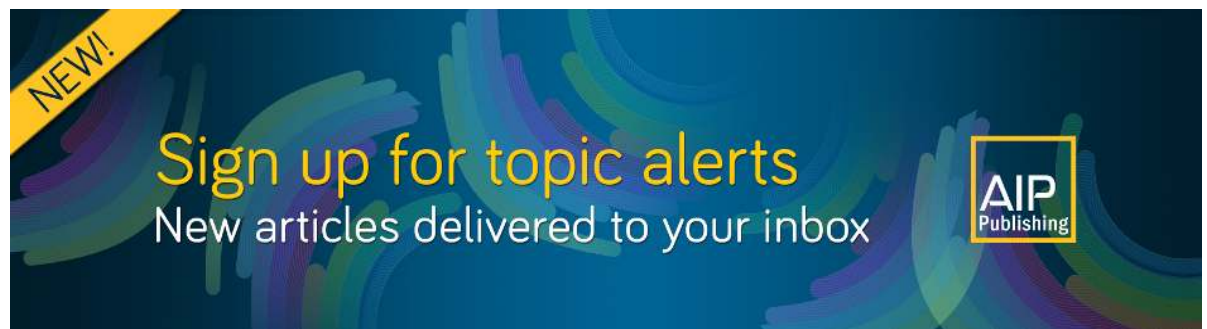
Physics of Fluids **32**, 083103 (2020); <https://doi.org/10.1063/5.0013725>

[Droplet deformation and breakup in shear flow of air](#)

Physics of Fluids **32**, 052109 (2020); <https://doi.org/10.1063/5.0006236>


[On respiratory droplets and face masks](#)

Physics of Fluids **32**, 063303 (2020); <https://doi.org/10.1063/5.0015044>



**NEW!**

Sign up for topic alerts  
New articles delivered to your inbox



# Enhanced stability of free viscous films due to surface viscosity

Cite as: Phys. Fluids 32, 082108 (2020); doi: 10.1063/5.0016282

Submitted: 3 June 2020 • Accepted: 22 July 2020 •

Published Online: 13 August 2020



Anjishnu Choudhury,<sup>1</sup> Venkatesh Kumar Paidi,<sup>2</sup> Sreeram K. Kalpathy,<sup>2</sup> and Harish N. Dixit<sup>1,a)</sup>

## AFFILIATIONS

<sup>1</sup>Indian Institute of Technology Hyderabad, Kandi, Sangareddy 502285, India

<sup>2</sup>Department of Metallurgical and Materials Engineering, Indian Institute of Technology Madras, Chennai 600036, India

**Note:** An earlier version of this article was uploaded on [arXiv:1902.11018](https://arxiv.org/abs/1902.11018), with a different title.

<sup>a)</sup>Author to whom correspondence should be addressed: [hdixit@mae.iith.ac.in](mailto:hdixit@mae.iith.ac.in)

## ABSTRACT

The stability of a thin liquid film bounded by two free surfaces is examined in the presence of insoluble surface-active agents. This study is broadly aimed at understanding enhanced stability of emulsions with the increasing surface concentration of surface-active agents. Surface-active agents not only cause gradients in surface tension but could also render surface viscosity to be significant, which could vary with surface concentration. We employ two phenomenological models for surface viscosity, a linear viscosity model and a nonlinear viscosity model. In the latter, surface viscosity diverges at a critical concentration, which is termed the “jamming” limit. We show that rupture can be significantly delayed with high surface viscosity. An analysis of the “jamming” limit reveals that  $\Gamma_i^{(nl)} > 3D/M$  provides a simple criterion for enhanced stability, where  $\Gamma_i^{(nl)}$ ,  $D$ , and  $M$  are the normalized initial surfactant concentration, disjoining pressure number, and Marangoni number, respectively. Nonlinear simulations suggest that high surface viscosity renders free films remarkably stable in the jamming limit, and their free surfaces behave like immobile interfaces consistent with experimental observations. Furthermore, it is shown that rupture times can be arbitrarily increased by tuning the initial surfactant concentration, offering a fluid dynamical route to stabilization of thin films.

Published under license by AIP Publishing. <https://doi.org/10.1063/5.0016282>

## I. INTRODUCTION

Surface-active agents are often used to modify surface rheological properties of dispersed media such as liquid foams, emulsions, and soap films. The interactions of these particle-laden interfaces are of great interest in several industrial applications such as foams and detergents, inks,<sup>1</sup> Pickering emulsions,<sup>2</sup> groundwater treatment,<sup>3</sup> and soil remediation.<sup>4</sup> Often surface-active agents become important through their inadvertent presence, for instance, as contaminants in the coating or printing process. They typically alter the wetting characteristics and hydrodynamics of a system by giving rise to interfacial stresses and affecting the surface properties of the system. The relevant surface properties of interest are surface tension, Marangoni effects, and concentration-dependent surface viscosity. A unified model that can characterize the interplay between these effects is necessary to truly predict the stability of such systems. As the subject of the present work, we formulate and solve a

mathematical model that addresses some of this interplay in a thin free liquid film, covered with insoluble surface-active agents at its free surface.

The configuration of a free liquid film has direct practical relevance to soap bubbles and cosmetic foams. A soap bubble is a thin spherical shell of water with air at a slightly elevated pressure trapped inside. Drainage of the aqueous layer due to gravity would lead to thinning and van der Waals forces, eventually causing rupture. Similar dynamics are seen in Pickering emulsions,<sup>5,6</sup> i.e., emulsions stabilized by adsorption of solid particles onto the interface between the dispersed phase and the continuous medium. Though the process is conceptually simple, the physics involved in determining the precise bubble breakup time is complicated. While high pressure inside the bubble can promote rupture, often leading to catastrophic breakup, the presence of surfactants creates Marangoni stresses at the fluid-liquid interface, which will delay the breakup time.<sup>7</sup> However, Marangoni stabilization alone may not provide

an adequate explanation for the remarkable stability exhibited by certain surfactant-stabilized emulsions, Pickering emulsions, and protein-based food colloids. The high surface viscosity at large surfactant concentrations can be a more significant factor that affects the breakup time. Therefore, the stability of bubbly suspensions and emulsions is a practical motivation for the model being studied here, though we do not make a distinction between the two. The model examined in the present work idealizes the space between two bubbles in an emulsion as a semi-infinite thin film of liquid in the longitudinal direction, with two free surfaces above and below it (see Fig. 1). The free surfaces are covered with a layer of surface-active agents (hereafter simply referred to as “surfactants”) that are insoluble in the bulk of the film. We neglect gravitational effects in the current study owing to the very thin films [ $O(100\text{ nm})$ ] considered here. Instead, long range van der Waals forces are included, and for simplicity, we ignore any stochastic effects such as the Brownian motion. Our configuration differs from that in the study of Naire *et al.*<sup>8,9</sup> and Braun *et al.*<sup>10</sup> who studied a vertical free film undergoing gravitational drainage, but given that very small gravitational effects could sometimes be important even in thin films, we believe our work may have relevance to draining films as well.

Before proceeding further, it is useful to highlight the existing literature on modeling stability of thin free liquid films. Several prior investigations<sup>11–15</sup> have modeled the dynamics of thin free films in the framework of lubrication theory, accounting for effects of capillarity, evaporation, condensation, and bulk viscosity. Among these, Hatzivramidis<sup>12</sup> was the earliest to explore the role of surfactants, which illustrated the competition between thermally and surfactant-induced Marangoni flows. In Hatzivramidis’s work, the dynamics of a free film were approximated by those of a wall film with half the thickness of a free film. A detailed presentation of the non-linear evolution equations using long-wave theory for a clean free film was first given by Erneux and Davis.<sup>14</sup> The concept was later extended to include insoluble surfactants at the surface by De Wit *et al.*,<sup>16</sup> in which they arrived at a system of three coupled non-linear evolution equations governing the film dynamics. Furthermore, this work was extended to soluble surfactants by Chomaz,<sup>17</sup> but he ignored the role of surface viscosity. It was not until the work by Edwards and Oron<sup>18</sup> and later by Naire *et al.*<sup>8,9</sup> and Braun *et al.*<sup>10</sup> that surface viscosity was incorporated into these models. Naire *et al.*<sup>9</sup> considered the configuration of a vertically draining

film, while Edwards and Oron<sup>18</sup> studied a horizontal film without surfactants and Marangoni effects. Using constant values of surface viscosity, Naire *et al.*<sup>8</sup> showed that the interface approaches an immobile limit in the limit of high surface viscosity. For draining interfaces with large surfactant concentrations, Braun *et al.*<sup>19</sup> assumed that the interface becomes completely immobile. We show later in the current study that regions of large particle concentration with high surface viscosity do indeed mimic an immobile interface. A model that includes Marangoni effects, surface viscosity, and bulk solubility of surfactants in horizontal free films was studied by Matar.<sup>20</sup>

In the present work, we show a crucial link between surface viscosity, surfactant concentration, interface mobility, and film stability, which is missing in the earlier literature. We present a plausible explanation to the following technologically and fundamentally relevant questions, with detailed fluid mechanical insights: “Why do many industrial emulsions possess an unusually long shelf-life?” “To what extent can surface viscosity aid in stabilizing such emulsions or liquid films?” To do so, we focus on horizontal non-draining films with surfactant-laden interfaces. We neglect the effect of surfactant solubility focusing primarily on the surface rheology. In particular, we use a model framework that allows surface viscosity to vary with surfactant concentration and show explicitly that if the former diverges at a sufficiently high concentration of surface-active particles, it is possible to immobilize the interface and achieve arbitrarily high breakup time for the film. Thus, we suggest that concentration-dependent surface viscosity mediated stabilization, a missing element in most earlier studies, offers a theoretical tool to analyze long shelf-life of surfactant-based emulsions. Our model primarily stems from a need to describe systems where surfactants or colloidal particles do exhibit large concentration variations on the interface, and such variations appear to be correlated with system stability. For example, Vignati *et al.*<sup>21</sup> have shown that densely covered Pickering emulsions with solid particle coverage as high as 50% or more exhibit low particle mobility on the interface as determined by measuring mean-squared displacement of particles. A similar result was obtained in the recent experiments of Mayarani *et al.*<sup>22</sup> who showed suppression of the coffee ring effect due to reduced mobility of particle-laden interfaces.

With recent improvements in rheometry, concentration-dependent surface viscosity has been measured accurately and is summarized in the review by Fuller and Vermant.<sup>23</sup> Edwards and

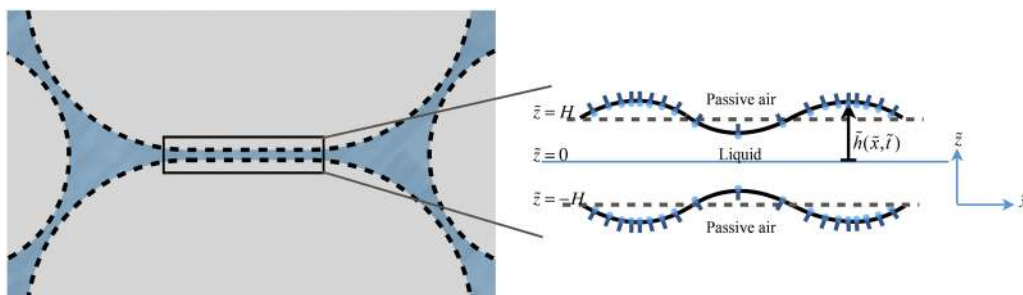


**FIG. 1.** Schematic of the problem geometry. A free film arises either in a typical soap bubble in air or between two bubbles or droplets in an emulsion. Bubbles deform as they approach each other forming a flat free film between them.

Wasan<sup>24</sup> developed a simple surface rheological model for a surfactant or particle-laden interface neglecting particle–particle interactions and showed that surface viscosity increases with surface concentration. Tambe and Sharma<sup>25</sup> extended this result to include interactions between particles and showed that surface viscosity is enhanced by orders of magnitude due to particle concentration and exhibits a divergent behavior as the concentration approaches a critical value. Danov *et al.*<sup>26</sup> showed that at sufficiently high surfactant concentrations, the interface appears to form a rigid shell accompanied by an enhancement in surface viscosity. Rising spherical bubbles and sedimenting drops covered with surfactants are known to have a drag coefficient different from that of a clean interface. In the limit of Stokes flows, such systems were modeled using the “spherical cap” approximation<sup>27</sup> where a part of the drop surface is assumed to be rigid (immobile), while the remainder of the drop is assumed to be devoid of surfactants,<sup>28</sup> similar to the immobile model of a draining film used by Braun *et al.*<sup>19</sup> Diffusion of surfactants on the interface makes the spherical cap approximation unrealistic, and one is expected to find a smooth variation in the concentration continuously reducing from the leeward to the windward side of the drop/bubble. Thus, in addition to Marangoni effects, we also introduce surface viscosity effects that depend on the local concentration of surfactants as demonstrated in prior experiments by Lopez and Hirska.<sup>29</sup> This allows us to have a continuous variation of the interfacial mobility consistent with diffusion effects of surfactants. A nonlinear phenomenological model describing this dependence is incorporated in the governing equations to construct a robust framework.

We adopt a scaling based on viscous forces balancing the intermolecular van der Waals interactions. The lubrication approximation is used to simplify the governing equations owing to the small aspect ratio of the free films. It is found that variable surface viscosity leads to new solutions for film evolution in the “dilute” limit when surface-active agents are sparsely distributed across the surface and the sensitivity of surface viscosity toward particle concentrations is weak. In addition, we also find that surfactants could potentially render a free film remarkably stable in the “jamming” limit.

We first derive a set of governing equations by non-dimensionalizing the Navier–Stokes equations and interfacial boundary conditions in Sec. II. We explore the linear stability of the system in Sec. III and apply perturbation techniques to reveal an important stability criterion in Sec. III A. A brief discussion of numerical methods used to solve the governing equations is provided in Sec. IV. This is followed by self-similar solutions found in the “dilute” regime in Sec. IV B 2 and important findings in the “jamming” limit in Sec. IV C. Finally, conclusions are made in Sec. V, connecting our results to prior experiments and findings.

## II. PROBLEM FORMULATION

### A. Problem geometry and governing equations

Figure 1 shows the idealized two-dimensional problem setup. A thin film of incompressible liquid, extending infinitely in the lateral direction, is bounded by a passive gas phase above and below it. The free surfaces on both sides are covered with surface-active agents that are assumed to be insoluble in the bulk of the film. These agents could either represent surfactants in the classical sense, significantly

affecting the liquid surface tension, or serve as colloidal particulates that alter the surface rheology. The film has mean thickness  $2H$  (dimensional), and the liquid has a bulk viscosity and density represented by  $\mu$  and  $\rho$  (both dimensional), respectively. The free surface is at a height  $\tilde{h}(\tilde{x}, \tilde{t})$ . Furthermore, we let  $\tilde{\sigma}_0$  denote the dimensional mean surface tension of the liquid film when the surface concentration of surfactants  $\tilde{\Gamma}$  is maintained at a fixed reference concentration  $\tilde{\Gamma}_0$ . Table I gives some realistic dimensional values for the various physical parameters used in our study.

Following prior works,<sup>14,16,20</sup> we will consider only the squeezing (or varicose) mode that is symmetric about the horizontal ( $\tilde{x}$ ) axis and is thus considered the most unstable mode. The dimensional momentum balance in the  $\tilde{x}$  and  $\tilde{z}$  directions and the continuity equation may be written as

$$\rho(\tilde{u}_t + \tilde{u}\tilde{u}_x + \tilde{v}\tilde{u}_z) = -(\tilde{P}_{\tilde{x}} + \tilde{\Phi}_{\tilde{x}}) + \mu(\tilde{u}_{\tilde{x}\tilde{x}} + \tilde{u}_{\tilde{z}\tilde{z}}), \quad (1)$$

$$\rho(\tilde{u}_t + \tilde{u}\tilde{v}_x + \tilde{v}\tilde{v}_z) = -(\tilde{P}_{\tilde{z}} + \tilde{\Phi}_{\tilde{z}}) + \mu(\tilde{v}_{\tilde{x}\tilde{x}} + \tilde{v}_{\tilde{z}\tilde{z}}), \quad (2)$$

$$\tilde{u}_{\tilde{x}} + \tilde{v}_{\tilde{z}} = 0. \quad (3)$$

Here,  $\tilde{u}$  and  $\tilde{v}$  denote the velocity components in  $\tilde{x}$  and  $\tilde{z}$  directions, while  $\tilde{P}$  is the fluid pressure. We have included a disjoining pressure term  $\tilde{\Phi}$  in our model, considering films to be thinner than  $\sim 100$  nm, where van der Waals forces are prevalent.<sup>18,30</sup> In the present work, we set  $\tilde{\Phi} = A/6\pi(2\tilde{h})^3$ , where  $A$  is the dimensional Hamaker constant representing van der Waals attraction between the two free surfaces separated by the liquid. The attractive van der Waals forces will be the prime destabilizing factor for the film. The dynamics of the surface-active species at the free surface neglecting their solubility in the bulk is governed by a convection–diffusion equation<sup>20</sup>

$$\tilde{\Gamma}_t + (\nabla_s \cdot \mathbf{n})\tilde{\Gamma}(\mathbf{n} \cdot \mathbf{u}) + \nabla_s \cdot (\mathbf{u}_s \tilde{\Gamma}) - D_s \nabla^2 \tilde{\Gamma} = 0. \quad (4)$$

Here,  $D_s$  is the surface diffusivity, treated as a constant,  $\nabla_s$  is the surface gradient operator,  $\mathbf{u}$  is the total velocity vector of the liquid,  $\mathbf{u}_s$  is the velocity vector along the free surface, and  $\mathbf{n}$  is the unit vector normal to the free surface. The various terms in (4) represent in order the local rate of change in surfactant concentration, the concentration variation resulting from local changes in the interfacial

TABLE I. Estimates of relevant physical parameters.

Parameter	Definition	Estimate	Units
$H$	Mean film thickness	$10^{-9}$ – $10^{-7}$	m
$M$	Liquid viscosity	$10^{-3}$	$\text{kg m}^{-1} \text{s}^{-1}$
$\rho$	Liquid density	$10^3$	$\text{kg m}^{-3}$
$A$	Hamaker constant	$10^{-21}$ – $10^{-19}$	J
$\tilde{\sigma}_0$	Surface tension of the clean film	$10^{-3}$ – $10^{-2}$	$\text{N m}^{-1}$
$\tilde{\Gamma}_0$	Mean surfactant concentration	$10^{-6}$	$\text{mol m}^{-2}$
$D_s$	Surface diffusion coefficient	$10^{-12}$ – $10^{-8}$	$\text{m}^2 \text{s}^{-1}$
$\tilde{\eta}_0$	Surface viscosity	$10^{-12}$ – $10^{-6}$	$\text{kg s}^{-1}$

area, the advective flux contribution, and the diffusive contribution, respectively. Note that the second term is a source-like contribution, expressed as a product of the mean interfacial curvature and the normal velocity.<sup>31</sup> The second and third terms may be combined and expressed as a single term  $\nabla_s \cdot (\tilde{\Gamma} \mathbf{u})$ . The split into two terms results when  $\mathbf{u}$  is decomposed into its components that are normal  $((\mathbf{n} \cdot \mathbf{u})\mathbf{n})$  and tangential  $(\mathbf{u}_s)$  to the free surface.<sup>27</sup>

The boundary conditions at the free surface ( $\tilde{z} = \tilde{h}(\tilde{x}, \tilde{t})$ ) are the normal stress continuity and the shear stress balance. The vector form of these equations in the presence of variable surface tension and surface viscosity effects is taken from Ref. 9, written as

$$-\mathbf{n} \cdot \|T\| \cdot \mathbf{n} = 2\kappa\tilde{\sigma} + 2\kappa(k^s + \mu^s)\nabla_s \cdot \mathbf{u}, \quad (5)$$

$$-\mathbf{t} \cdot \|T\| \cdot \mathbf{n} = \mathbf{t} \cdot \nabla_s \tilde{\sigma} + (k^s + \mu^s)\mathbf{t} \cdot \nabla_s \nabla_s \cdot \mathbf{u} + \mathbf{t} \cdot \nabla_s (k^s + \mu^s)\nabla_s \cdot \mathbf{u}, \quad (6)$$

where  $\mathbf{t}$  is the unit vector tangent to the free surface,  $T$  is the stress tensor, and  $\|T\|$  denotes its jump across the liquid–air interface. Thus, the left-hand sides of (5) and (6) denote, respectively, the net jump in stress normal to and tangential to the air–liquid interface. The dilatational ( $k^s$ ) and shear ( $\mu^s$ ) components of surface viscosities occur in additive pairs in a 2D system and will hereafter be written in terms of a single parameter,  $\tilde{\eta} = (k^s + \mu^s)$  in the rest of this paper. Derivation of these equations that is beyond the scope of this paper can be found in books by Slattery *et al.*<sup>32</sup> and Brenner.<sup>33</sup> These equations are a simple extension of the Newtonian interface model for a constant surface viscosity first derived by Scriven.<sup>34</sup> The first term on the right-hand side (RHS) of (5) denotes the capillary pressure,  $\kappa$  being the mean interfacial curvature and  $\tilde{\sigma}$  being the dimensional surface tension of the liquid. The second term is a normal component of the viscous resistance to the deformation of the surface arising from both dilatational and shear surface viscosities. Its tangential component is present in the second term on the RHS of (6), the tangential stress balance condition. In addition, (6) also contains the contributions from Marangoni stress (the first term on the RHS) and the spatial variation in surface viscosity (the last term on the RHS). The latter occurs due to variations in surfactant concentration  $\tilde{\Gamma}$ , and the specific functional forms used to describe how  $\tilde{\eta} = (k^s + \mu^s)$  varies with  $\tilde{\Gamma}$  will be shown in Sec. II B. The simplified scalar versions of (5) and (6) in dimensional and dimensionless forms are shown in Appendixes A 1 and A 2. The other conditions that complete the system are the kinematic condition at the free surface and the symmetry condition at the centerline ( $\tilde{z} = 0$ ). These are written as

$$\tilde{h}_t + \tilde{u}\tilde{h}_x = \tilde{v} \quad (\text{kinematic}), \quad (7)$$

$$\tilde{u}_z = 0 \quad \text{and} \quad \tilde{v} = 0 \quad (\text{squeezing mode symmetry}). \quad (8)$$

### B. Scalings and non-dimensionalization

The scalings for the different variables are explained next, where symbols with the tilde ( $\sim$ ) decoration denote dimensional versions. The spatial coordinates  $\tilde{z}$  and  $\tilde{x}$  are scaled as

$$z = \frac{\tilde{z}}{H}, \quad x = \frac{\tilde{x}}{L}, \quad (9)$$

where  $L$  is the characteristic length along  $\tilde{x}$  (e.g., the wavelength of a typical interfacial perturbation). We further assume that  $\epsilon = H/L \ll 1$ , i.e., a small aspect ratio film, which would permit us to employ the lubrication approximation. The velocity components and the fluid pressure are scaled as follows:

$$u = \frac{\tilde{u}}{A/6\pi\mu\epsilon L^2}, \quad v = \frac{\tilde{v}}{A/6\pi\mu L^2}, \quad P = \frac{\tilde{P}}{A/6\pi\epsilon L^3}. \quad (10)$$

The scalings in (10) reflect a balance between viscous stresses and the disjoining pressure gradient due to van der Waals forces. We note that our choice of scalings is different from that in Ref. 20 (extensional viscous stresses  $\sim$  Marangoni stresses) and would be more apt for ultra-thin films ( $\leq 100$  nm).<sup>18,30,35</sup> The natural choice for the characteristic timescale is the ratio of the characteristic scales of velocity and length. Thus, the dimensionless time variable is expressed as

$$t = \frac{\tilde{t}}{6\pi\mu\epsilon L^3/A}. \quad (11)$$

Since surface properties depend on surfactant concentration, suitable scales are needed for the concentration, surface tension, and surface viscosity given by

$$\Gamma(x, t) = \frac{\tilde{\Gamma}(\tilde{x}, \tilde{t})}{\tilde{\Gamma}_{\text{ref}}}, \quad \sigma(x, t) = \frac{\tilde{\sigma}(\tilde{x}, \tilde{t})}{\tilde{\sigma}_{\text{ref}}}, \quad \eta(x, t) = \frac{\tilde{\eta}(\tilde{x}, \tilde{t})}{\tilde{\eta}_{\text{ref}}}. \quad (12)$$

The reference surface tension,  $\tilde{\sigma}_{\text{ref}}$ , is taken to be the value of surface tension for a clean interface that is devoid of any surface concentration [i.e., in the limit  $\tilde{\Gamma}(\tilde{x}, \tilde{t}) \rightarrow 0$ ]. The surface viscosity,  $\tilde{\eta}$ , is scaled with  $\tilde{\eta}_{\text{ref}}$ , the choice of which depends on the type of model used for  $\tilde{\eta}$  as explained below. The reference surfactant concentration ( $\tilde{\Gamma}_{\text{ref}}$ ) could be an initial equilibrium surface concentration in the dilute limit ( $\tilde{\Gamma}_{\text{dil}}$ ), or a critical concentration of colloidal surface-active agents in a jammed-state interface ( $\tilde{\Gamma}_{\text{max}}$ ).

Several dimensionless characteristic numbers appear upon rewriting (1)–(8) using the scalings mentioned above. These are summarized in Table II along with their typical order of magnitude estimates based on physical values given in Table I. Among these, the parameters representing dominant effects are  $\mathcal{B}$  (non-dimensional surface viscosity) and  $\mathcal{D}$  (non-dimensional ratio of disjoining forces to surface tension forces). Furthermore, the Marangoni number  $M$  and the surface viscosity gradient parameter,  $\beta$ , represent the variation of surface tension and surface viscosity with surfactant concentration. For simplicity, we assume a linear variation with concentration for surface tension, given by

$$\sigma = 1 - M\Gamma(x, t). \quad (13)$$

To shed light on the effect of surface viscosity and its dependence on concentration, especially near the jamming limit, we use two phenomenological viscosity models: (i) linear viscosity model (LVM) given by

$$\eta = 1 + \beta[\Gamma(x, t) - 1] \quad (14)$$

and (ii) nonlinear viscosity model (NVM) given by

$$\eta = \frac{1}{[1 - \Gamma(x, t)]^\alpha}. \quad (15)$$

**TABLE II.** Estimates of non-dimensional system parameters evaluated using the characteristic velocity scale and dimensional estimates from Table I. Reference quantities such as  $\tilde{\eta}_{ref}$ ,  $\tilde{\sigma}_{ref}$ , and  $\tilde{\Gamma}_{ref}$  are given in Table I.

Parameter	Definition	Order of magnitude estimates
$\epsilon = \frac{\tilde{h}_0}{L}$	Aspect ratio	$10^{-3}-10^{-2}$
$\mathcal{B} = \frac{\tilde{\eta}_{ref}}{\mu h_0}$	Boussinesq number	$10^{-1}-10^1$
$\mathcal{D} = \frac{A}{6\pi\tilde{\sigma}_{ref}\epsilon L^2}$	Disjoining pressure number	$10^{-3}-10^{-2}$
$M = \frac{\tilde{\Gamma}_{ref}}{\tilde{\sigma}_{ref}} \left( \frac{\partial\tilde{\sigma}}{\partial\tilde{\Gamma}} \right)$	Marangoni number	$0-5 \times 10^{-3}$
$\beta = \frac{\tilde{\Gamma}_{ref}}{\tilde{\eta}_{ref}} \left( \frac{\partial\tilde{\eta}}{\partial\tilde{\Gamma}} \right)$	Surface viscosity gradient number	0-1
$Pe = \frac{A}{6\pi\mu h_0 D_s}$	Peclet number	$10^{-1}-10^2$
$Re = \frac{\rho A}{6\pi\mu^2\epsilon\tilde{h}_0}$	Reynolds number	$10^{-2}-1$

The relevant characteristic scales for surface tension, concentration, and viscosity for the LVM and NVM are given in Table III.

The form of the LVM given in Eq. (14) allows us to define a linear variation in surface viscosity at any non-zero concentration. This enables us to establish equivalence between the two viscosity models at a specific reference concentration as discussed in Appendix B. In general, a linear viscosity model is best suited to an interface with a sparse distribution of surfactants or particles. The reference concentration  $\tilde{\Gamma}_{ref}$  can be interpreted as a reference equilibrium concentration in the dilute limit. For the nonlinear model (15), the jammed state concentration value  $\tilde{\Gamma}_{max}$  of the system would intuitively be the suitable non-dimensionalizing factor for  $\tilde{\Gamma}$  as the surface viscosity is expected to diverge in the jammed state, analogous to bulk viscosity.<sup>36-38</sup> The nonlinear model employed in the current study agrees well with the theoretical prediction of Tambe and Sharma<sup>25</sup> for a particle-laden interface shown in Fig. 2. Note that the nonlinear viscosity model (NVM) can be reduced to a linear model in the limit of dilute surfactant concentration ( $\tilde{\Gamma}_{dil} \ll \tilde{\Gamma}_{max}$ ). In this limit, the exponent  $\alpha$  in (15) is related to the surface viscosity gradient parameter  $\beta$

**TABLE III.** Characteristic scales for concentration, surface tension, and surface viscosity. The surface tension at zero concentration is used as a reference for both the viscosity models. For the LVM, the dilute limit  $\tilde{\Gamma}_{dil}$  can be any value of  $\tilde{\Gamma}$  that satisfies  $\tilde{\Gamma} \leq \tilde{\Gamma}_{max}/(\alpha + 1)$  (see Appendix B for more details). The subscript “0” indicates that the parameter is defined for a clean interface where the concentration is zero.

Model	$\tilde{\Gamma}_{ref}$	$\tilde{\sigma}_{ref}$	$\tilde{\eta}_{ref}$
LVM	$\tilde{\Gamma}_{dil}$	$\tilde{\sigma}_0$	$\tilde{\eta}_{dil}$
NVM	$\tilde{\Gamma}_{max}$	$\tilde{\sigma}_0$	$\tilde{\eta}_0$

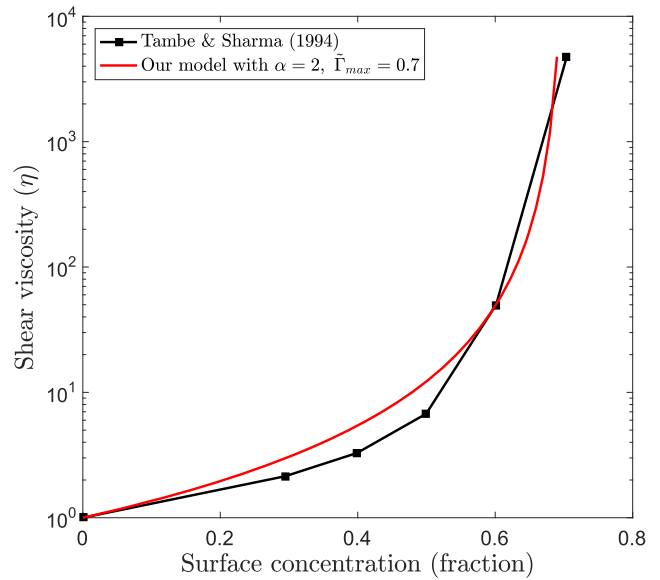


**FIG. 2.** Effect of surface concentration on surface viscosity. A black line with markers represents theoretical predictions from the micro-mechanical model of Tambe and Sharma,<sup>25</sup> and the red curve is a fit of the NVM.

in (14) by the relation

$$\frac{\tilde{\Gamma}_{dil}}{\tilde{\Gamma}_{max}} = \frac{\beta}{\alpha + \beta} = \frac{\Gamma_i^{(nl)}}{\Gamma_i^{(l)}}, \tag{16}$$

where  $\Gamma_i^{(l)}$  and  $\Gamma_i^{(nl)}$  denote the respective non-dimensional base-state values in the linear and nonlinear models. Further details of the validity and derivation of equivalence in surface viscosity models are given in Appendix B. We also note that the system with the NVM reduces to a system with constant surface viscosity when  $\Gamma \rightarrow 0$ , in accordance with a Newtonian viscosity for a clean interface discussed in the work of Scriven.<sup>34</sup>

The disjoining pressure number,  $\mathcal{D}$  in Table II, defined as  $\mathcal{D} = A/6\pi\sigma_0\epsilon L^2$  has been deliberately scaled to contain  $\epsilon$ , so that capillary effects are retained in the normal stress boundary condition, as also described in Appendix A 1. It represents the ratio of inter-molecular van der Waals interactions to surface tension forces. A disjoining pressure interpretation of the capillary effects is apt as it represents the overall wetting characteristics of the thin-film system, as has been done in an earlier work.<sup>39</sup> With respect to Marangoni and surface viscosity effects, we restrict ourselves to the default regime examined in prior works<sup>16,20</sup> in which both Marangoni effects and surface viscosity only appear in the first order correction of the tangential stress balance condition. Accordingly, if  $M$  is an  $O(1)$  quantity, a “weak Marangoni” limit is defined by rescaling it as  $M = \epsilon^2 \tilde{M}$ , where the new  $O(1)$  parameter is  $\tilde{M}$ . Then, Marangoni effects would drop out in the lubrication limit when  $O(\epsilon^2)$  terms are ignored. The idea is elaborated further in Appendix C. Following the definition of  $\sigma$  in (13), the weak Marangoni limit would imply, at leading order,

$$\sigma = 1 \quad \text{and} \quad \sigma_x = 0. \tag{17}$$

For the surface viscosity,  $\eta$  is retained as an  $O(1)$  quantity, but it would still appear only in the first (and higher) order corrections to the stress balance conditions as shown by Matar.<sup>20</sup> To explore the strong surface viscosity regime (see Appendix C),  $\eta$  may be rescaled such that it is retained at leading order and the boundary conditions are self-consistent. However, as  $\epsilon$  (aspect ratio) can be made arbitrarily small, presenting the surface viscosity terms at  $O(\epsilon)$  stress balance conditions (as in the present formulation) could still be deemed acceptable despite the diverging nature of the NVM.

### C. Evolution equations

With the scalings presented in Sec. II B, the governing equations (1)–(3) reduce to the following when only the zeroth (leading) order terms are considered, denoted with the superscript 0:

$$u_{zz}^{(0)} = 0, \tag{18}$$

$$P_z^{(0)} = v_{zz}^{(0)}, \tag{19}$$

$$u_x^{(0)} + v_z^{(0)} = 0. \tag{20}$$

Rewriting the symmetry conditions in (8) at  $z = 0$  gives

$$u^{(0)} = c(x, t), \tag{21}$$

$$v^{(0)} = -c_x z, \tag{22}$$

where  $c(x, t)$  is still an unknown function independent of  $z$ . We see in (21) that the horizontal velocity is a plug flow varying spatially and temporally. The leading order normal stress balance (see Appendix A 1) is written as

$$-P^{(0)} = \mathcal{D}^{-1} h_{xx} + 2h_x u_z - 2v_z. \tag{23}$$

Integrating (19), comparing it with (23), and substituting (21) and (22), we obtain

$$P^{(0)} = -2c_x - \mathcal{D}^{-1} h_{xx}^{(0)}. \tag{24}$$

The leading order tangential stress balance (see Appendix A 2), on the other hand, simplifies to [using (17)]

$$u_z^{(0)} = \mathcal{D}^{-1} \sigma_x = -\epsilon^2 \mathcal{D}^{-1} M \Gamma_x^{(0)} = 0. \tag{25}$$

This is also consistent with (21). The kinematic condition (7) and the surfactant transport equation (4) provide two nonlinear evolution equations for  $h^{(0)}$  and  $\Gamma^{(0)}$ , with  $c(x, t)$  still undetermined. As discussed by De Wit *et al.*<sup>16</sup> and Matar,<sup>20</sup> the system can be completed only through a third equation obtained by considering the first order corrections of (18) and (25) (refer to Appendixes A 2 and A 3). To these, we substitute (14) or (15) to account for variable viscosity.

The final system of three nonlinear evolution equations reads

$$h_t + (ch)_x = 0, \tag{26}$$

$$\Gamma_t + (c\Gamma)_x = \frac{\Gamma_{xx}}{Pe}, \tag{27}$$

$$\begin{aligned} & Re(c_t + cc_x) - \mathcal{D}^{-1} h_{xxx} - \frac{3}{8h^4} h_x \\ &= 4 \frac{(hc_x)_x}{h} + \mathcal{B}(\eta) \frac{c_{xx}}{h} + \mathcal{B} \left( \frac{d\eta}{d\Gamma} \right) \frac{c_x \Gamma_x}{h} - \mathcal{D}^{-1} M \frac{\Gamma_x}{h}. \end{aligned} \tag{28}$$

The above set of evolution equations is valid for both linear and non-linear viscosity models with only the value of  $\eta$  and its variation chosen based on either (14) or (15). Non-dimensional parameters such as  $Re$ ,  $Pe$ ,  $M$ ,  $\mathcal{B}$ , and  $\mathcal{D}$  are defined in Table II. The superscript 0 has been omitted in (26)–(28) and in the remainder of this paper for easy readability. We note that these equations reduce to those derived by De Wit *et al.*<sup>16</sup> in the limit  $\mathcal{B} = 0$  and to those derived by Matar<sup>20</sup> when we set  $d\eta/d\Gamma = 0$ , in the absence of surfactant solubility. The key augmentation of the present work is the term containing  $d\eta/d\Gamma$ , which plays a role through the tangential stress at first order.

While (26) and (27) have the more familiar form of evolution equations at leading order, (28) has been derived by considering the first order correction [ $O(\epsilon^2)$ ] of the velocity  $u$ . Physically, (28) may be construed as a form of conservation of linear momentum applicable at first order. Its first term on the left-hand side (LHS) contains the material derivative of the velocity function  $c$ , with the  $cc_x$  term representing the convective acceleration contribution. The second and third terms on the LHS can be reformulated as a pressure gradient, as in the typical Navier–Stokes equations, if we identify the pressure field as  $\mathcal{P} = \mathcal{D}^{-1} h_{xx} - \frac{1}{8h^3}$ , which is a sum of contributions from surface tension (capillary pressure) and the van der Waals forces (disjoining pressure). On the RHS, the first term is an equivalent “viscous” stress term, with  $h$  and  $h_x$  accounting for variable viscous resistance offered by the fluid particles at first order as the film undergoes local thinning. The factor of 4 has been noted as the ratio of the elongational to the shear viscosity in planar Newtonian viscous flows, and  $4h$  is termed the “Trouton viscosity.”<sup>14</sup> The remaining terms on the RHS arise, respectively, from the surface-viscous resistance, its dependence on the surfactant concentration, and the surface tension gradients or Marangoni flow. The latter has a finite contribution to the tangential stress only at first order in the “weak Marangoni” limit, as explained in Appendix C. The appearance of the concentration dependence of surface viscosity in (28) suggests that spatial gradients in surface viscosity do generate linear momentum flux at first order.

### III. LINEAR STABILITY ANALYSIS

We linearize the system of three nonlinear equations (26)–(28), by perturbing the dependent variables about a uniform base state as follows:

$$h(x, t) = \frac{1}{2} + \hat{h} e^{(ikx+st)}, \tag{29}$$

$$\Gamma(x, t) = \Gamma_i + \hat{\Gamma} e^{(ikx+st)}, \tag{30}$$

$$c(x, t) = \hat{c} e^{(ikx+st)}. \tag{31}$$

Here,  $s$  is the growth rate and  $k$  is the wavenumber of the perturbation. Using standard linear stability analysis, the following dispersion relation is obtained for the linear and nonlinear surface viscosity

models:

$$\begin{aligned}
 & s^3 + s^2 k^2 \left( \frac{1}{Pe} + \frac{4}{Re} + \frac{2\mathcal{B}\eta_i}{Re} \right) \\
 & + sk^2 \left( \frac{4k^2}{PeRe} + \frac{\mathcal{D}^{-1}k^2}{2Re} - \frac{3}{Re} + \frac{\mathcal{D}^{-1}M\Gamma_i}{Re} + \frac{2\mathcal{B}\eta_i k^2}{PeRe} \right) \\
 & + \frac{k^4}{PeRe} \left( \frac{\mathcal{D}^{-1}k^2}{2} - 3 \right) = 0,
 \end{aligned} \tag{32}$$

where  $\Gamma_i$  is the non-dimensional base-state surface concentration and can be taken to be either  $\Gamma_i^{(l)}$  or  $\Gamma_i^{(nl)}$  depending on whether the LVM or NVM is used. It has to be noted that only a base-state value of surface viscosity affects linear stability whose value is given by  $\mathcal{B}\eta_i$ , where  $\eta_i$  is calculated by either (14) or (15) at surface concentration equal to  $\Gamma_i$  and  $\mathcal{B}$  is the Boussinesq number given in Table II. Since variable surface viscosity effects do not appear in the linear stability analysis, the above dispersion relationship reduces to that in the constant viscosity study of Matar.<sup>20</sup> In addition, the above dispersion relation is also in agreement with that in earlier studies<sup>14,16</sup> in the absence of surface viscosity, i.e.,  $\eta_i = 0$ . We show later that the functional form of surface viscosity models plays an important role in nonlinear evolution of the thin film.

The dispersion curves for three different values of “effective viscosity” corresponding to a base-state surfactant concentration ranging from the dilute to the concentrated limit are shown in Fig. 3(a). Other parameter values are chosen from Table II and are similar to values chosen by Matar.<sup>20</sup> All the curves exhibit a fastest growing mode,  $k_{max}$ , and a cut-off wavenumber,  $k_c$ , given by

$$k_c = \sqrt{6\mathcal{D}}, \tag{33}$$

above which the film is stable. The qualitative trends seen in the dispersion curves were similar to observations reported in earlier works.<sup>14,16,20</sup> In all our cases, the dispersion relation is a cubic polynomial with one growing root and two decaying roots, and only the growing root is shown in the dispersion curves in all the plots below.

For the sake of completeness, the role of various non-dimensional parameters is briefly discussed below. Separate dispersion curves for each of these cases can be easily generated and

are discussed in the work of Matar.<sup>20</sup> A decrease in  $\mathcal{D}$  results in greater opposition from surface tension toward film breakup and a smaller driving force from intermolecular van der Waals attractions, leading to reduction in maximum growth rates. As regards  $Pe$ , a higher surface diffusivity of the surfactants (lower values of  $Pe$ ) diminishes gradients in surfactant concentrations to destabilize the film. Marangoni stresses are generated due to variations in surface concentrations, which leads to variations in surface tension. This creates a mass flux along the interface, which drives the fluid into regions of high surface tension or low surfactant concentration that exists where the interface dips toward rupture. The mass flux reduces the rate at which the interface recedes, thus reducing the growth rate. A detailed discussion on Marangoni-induced stabilization is provided in the work of De Wit *et al.*<sup>16</sup> The role of  $Re$  is the most enigmatic among all parameters and has not been discussed in detail in earlier works. Interestingly, the  $Re \rightarrow 0$  limit is singular and does not give the same result as  $Re = 0$ . This is also evident from the growth rate curves given in Fig. 3(b), which show that the dominant wavenumber moves toward lower values of  $k$  with the decreasing Reynolds number. This is accompanied by a steep rise in the dispersion curve near  $k = 0$  with a small increase in the dominant growth rate. This can be explained by noting that as  $Re$  decreases, viscosity is most effective at suppressing growth at small scales. Hence, regions of dominant growth are pushed toward large scales or low wavenumber. However, the physical mechanism behind the increase in the growth rate with the decreasing  $Re$  is unclear, and a more careful study is warranted.

The effects of surface viscosity are determined by the parameters  $\mathcal{B}$ ,  $\beta$ ,  $\alpha$ , and  $\Gamma_i$ . However, as already discussed, the dispersion relation only depends upon the effective initial surface viscosity. We can tune the above four parameters and get the same effective surface viscosity for different models used. The choice of model used depends upon the system under study. As far as linear stability is considered, we vary the effective surface viscosity ( $\mathcal{B}\eta_i$ ) and observe the behavior of the dispersion relation (32) as shown in Fig. 3(a). At higher values of surface viscosity, there is an overall decrease in the growth rate, but the dispersion curves show a boundary layer-like structure at small wavenumbers. The structure of the dispersion

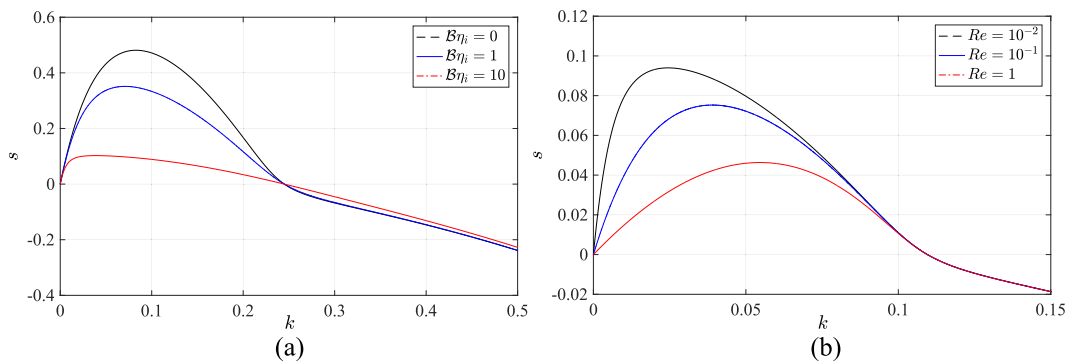


**FIG. 3.** Dispersion curves with the (a) varying effective surface viscosity,  $\mathcal{B}\eta_i$ , with fixed  $Re = 10^{-1}$  and (b) varying Reynolds number,  $Re$ , with fixed  $\mathcal{B} = 10^{-1}$  and  $\Gamma_i^{(l)} = 2$ . Other parameters are fixed as  $Pe = 1$ ,  $\mathcal{D} = 10^{-2}$ ,  $M = 10^{-3}$ .



curves near the jamming limit where surface viscosity assumes very large values is discussed in Sec. III A.

### A. The “jamming limit”

In this section, we show that it is possible to obtain a simple perturbation solution to the dispersion relation (32) using the NVM case, (15), in the limit of large surfactant concentration, i.e., for  $\Gamma_i^{(nl)} \rightarrow 1$ . In this limit, the surfactant concentration approaches the jamming limit and the mobility of surfactant molecules reduces to zero. It will be shown later (see Sec. IV C) that the tangential velocity indeed reduces to zero as  $\Gamma_i^{(nl)} \rightarrow 1$ . This limit leads to diverging surface viscosity terms in (32) exhibiting a distinct boundary layer-like structure. It is shown below that the nature of the cubic equation changes in the jamming limit. To proceed with the perturbation analysis, it is convenient to define a small parameter,  $\delta = (1 - \Gamma_i^{(nl)})^\alpha$ . As  $\Gamma_i^{(nl)} \rightarrow 1$ ,  $\delta \rightarrow 0$ . The dispersion relation for the NVM can then be rewritten in terms of  $\delta$  as

$$\delta s^3 + s^2[\delta a_1(k) + a_2(k)] + s[\delta a_3(k) + a_4(k)] + \delta a_5(k) = 0, \quad (34)$$

where the coefficients  $a_1$  to  $a_5$  are functions of  $k$  and can be obtained by comparing (34) with (32),

$$a_1(k) = \left(\frac{1}{Pe} + \frac{4}{Re}\right)k^2, \quad (35)$$

$$a_2(k) = \frac{2B}{Re}k^2, \quad (36)$$

$$a_3(k) = \left(\frac{D^{-1}M\Gamma_i^{(nl)}}{Re} - \frac{3}{Re} + \frac{4}{PeRe}k^2 + \frac{D^{-1}}{2Re}k^2\right)k^2, \quad (37)$$

$$a_4(k) = \frac{2B}{PeRe}k^4, \quad (38)$$

$$a_5(k) = \left(\frac{D^{-1}k^2}{2} - 3\right)\frac{k^4}{PeRe}. \quad (39)$$

In the limit  $\delta \rightarrow 0$ , Eq. (34) is a standard singular perturbation problem for the growth rate  $s$ . Figure 4(a) shows plots of the sole positive root of (34) for different values of  $\delta$ . It is apparent that the growth rate  $s$  scales with  $\delta$  and singular root appears in the region  $k \leq \delta$ . We therefore define a rescaled growth parameter  $Y = s/\delta$ , so that Eq. (34) now becomes

$$\delta^3 Y^3 + Y^2[\delta^2 a_1(k) + \delta a_2(k)] + Y[\delta a_3(k) + a_4(k)] + a_5(k) = 0. \quad (40)$$

A standard expansion in  $\delta$  in the form  $Y^{(o)} = Y_0^{(o)} + \delta Y_1^{(o)} + \dots$  results in two regular roots in the outer region, i.e.,  $k \gg \delta$ . Focusing on the root that is unstable, we obtain

$$Y_0^{(o)} = -\frac{a_5}{a_4}, \quad (41)$$

$$Y_1^{(o)} = -\frac{a_2 a_5^2}{a_4^3} + \frac{a_3 a_5}{a_4^2}. \quad (42)$$

To obtain the singular root in the inner region  $0 \leq k \leq \delta$  that has a boundary layer-like structure, we define a rescaled variable  $X = k/\delta$ , where  $X \sim O(1)$ . The solution to the inner region in terms of this rescaled variable at leading order is

$$Y_0^{(i)} = -\frac{b_2}{2} + \frac{1}{2}\sqrt{b_2^2 - 4b_3}, \quad (43)$$

where  $b_2 = \frac{2B}{Re}X^2$ ;  $b_3 = \left(\frac{D^{-1}M\Gamma_0}{Re} - \frac{3}{Re}\right)X^2$ . Figure 4(b) shows a

comparison of the inner solution  $Y_0^{(i)}$  (dotted-dashed line), the outer solution  $Y_0^{(o)}$  (dashed line), and the numerical root  $Y$  (solid line) obtained from (40). Examining (43), it can be shown that the necessary condition for stable growth rates ( $Y_0^{(i)} < 0$ ) is  $b_3 > 0$ . Hence,

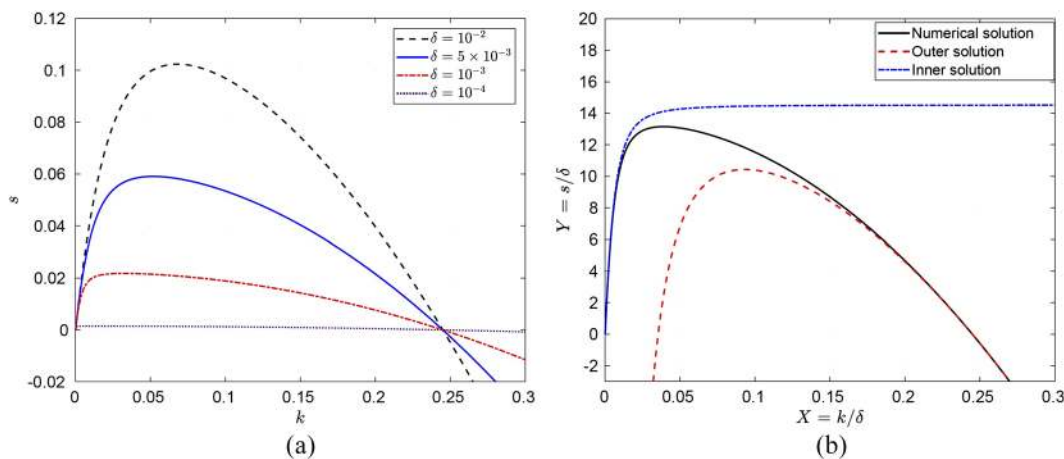


**FIG. 4.** (a) Unstable root for the dispersion relation (34) with the varying  $\delta = (1 - \Gamma_i^{(nl)})^\alpha$ . The growth rate scales with  $\delta$ , and the  $s(k)$  curve exhibits a sharp gradient near  $k \rightarrow 0$ . (b) Inner  $Y^{(i)}$  (dotted-dashed line) and outer  $Y^{(o)}$  (dashed line) perturbation solutions along with the full dispersion relation from Eq. (40) compared with numerical roots (solid line). Other parameters are fixed as  $D^{-1} = 100$ ,  $M = 10^{-3}$ ,  $Pe = 1$ ,  $Re = 10^{-2}$ ,  $\alpha = 2$ .

we arrive at a necessary condition for obtaining stable modes in the space  $0 \leq k \leq \delta$ ,

$$\Gamma_i^{(nl)} > \frac{3}{\mathcal{D}^{-1}M}. \tag{44}$$

However, this criterion is solely extracted from the inner solution. When we examine the complete numerical solution, we find that there is a change in the nature of the dispersion curves with the increasing surfactant concentration. If the above criterion is satisfied, it is found that the growth rate goes to zero in the small- $k$  region, but a region of dominant growth exists for larger values of  $k$ . The growth rates can assume very small but positive values even when the above criterion is satisfied. The maximum growth rates are found to vary over three orders of magnitude: from  $s \sim O(1)$  to  $s \sim O(10^{-3})$  in the limit  $0 \leq k \leq \delta$ . We can therefore define a critical concentration  $\Gamma_c = 3/\mathcal{D}^{-1}M$  for stability in the long-wave limit. Any value of  $\Gamma_i^{(nl)} > \Gamma_c$  should result in enhanced stability. Examining the system parameters in real physical systems, we find that  $\mathcal{D}^{-1}M \sim O(10^{-1})$  in real systems, suggesting that though foams can be stable for a long duration, indefinite stability is not guaranteed. This is consistent with the observation by Kloek *et al.*<sup>40</sup> who studied bubble dissolution with complex interfacial and bulk rheologies. It is easy to derive a simple relationship between the amplitude of tangential velocity at the interface,  $\hat{c}$ , and the height perturbation,  $\hat{h}$ , using the kinematic condition (29),

$$\hat{c} = \frac{is}{kh_0} \hat{h}. \tag{45}$$

The above relationship suggests that the tangential velocity at the interface,  $c(x, t)$ , has a phase-difference with the interface height,  $h(x, t)$ , since  $\hat{c}$  is a complex number. Since the interface height is symmetric about the rupture location, the tangential velocity is anti-symmetric. This result is unsurprising because as the interface height reduces toward rupture, the fluid is driven away from the rupture location. An important outcome of the above analysis is that the growth rate scales with the small parameter  $\delta$  in the jamming limit. This dependence can be written in the simple form

$$s = \left(1 - \Gamma_i^{(nl)}\right)^\alpha F(Re, Pe, \mathcal{D}, M, \mathcal{B}), \tag{46}$$

where we have used the definition of  $\delta$  and the functional dependence on other parameters,  $F$ , is not reproduced for simplicity. Substituting  $s$  into (45), we get

$$\hat{c} = \frac{iF\left(1 - \Gamma_i^{(nl)}\right)^\alpha}{kh_0} \hat{h}. \tag{47}$$

As  $\Gamma_i^{(nl)} \rightarrow 1$ , it is clear that  $c(x, t) \rightarrow 0$ , thus rendering the interface immobile in the jammed limit. Both the anti-symmetric nature of the tangential velocity and the approach to the immobile limit are confirmed through full numerical solutions of Eqs. (26)–(28) in Sec. IV.

## IV. NONLINEAR EVOLUTION

### A. Numerical methods

The nonlinear evolution and dynamics of the free film were studied by numerically solving the set of partial differential

equations (26)–(28) for a range of parameter values. A Fourier pseudo-spectral (FPS) method is used to solve these PDEs, since it is most suited to handle periodic boundary conditions. Discretization of the spatial derivatives in the Fourier domain reduces the set of PDEs to ordinary differential equations.<sup>41</sup> Time marching is done using an implicit Adams–Moulton method (trapezoidal rule) using the MATLAB function *fsolve* to solve the linearized equations in the Fourier space. An adaptive time stepping  $\Delta t \propto \kappa^{-1}$  (curvature) is also implemented to capture the dynamics at later times, when the evolution proceeds much faster. The initial conditions used in our simulations are as follows:

$$h(x, 0) = \frac{1}{2} + 0.01 \cos\left(\frac{2\pi x}{\lambda}\right), \tag{48}$$

$$\Gamma(x, 0) = \Gamma_i + \Delta\hat{\Gamma} \cos\left(\frac{2\pi x}{\lambda}\right), \tag{49}$$

$$c(x, 0) = 0, \tag{50}$$

where  $\lambda = 2\pi/k_{\max}$  is the fastest growing wavelength, determined from linear stability analysis. The perturbation amplitude for surfactant concentration  $\Delta\hat{\Gamma}$  is set using

$$\Delta\hat{\Gamma} = \frac{s_{\max}\Gamma_i\Delta\hat{h}}{h_0(s_{\max} + k^2/Pe)}, \tag{51}$$

which is obtained from linear stability analysis. Here, we use  $\Gamma_i^{(l)} = 2$  and  $\Gamma_i^{(nl)}$  varying between 0 and 0.95 for the linear and nonlinear models, respectively. Furthermore, we set  $h_0 = 0.5$ ,  $\Delta\hat{h} = 0.01$ , with  $s_{\max}$  being the maximum value of the growth rate predicted by the linear theory, at  $k = k_{\max}$ . The time steps used in the initial stages are of the order  $\Delta t \sim O(10^{-1})$  and reduce to  $\Delta t \sim O(10^{-3})$  at the later stages of our numerical simulations. The spatial domain is discretized into 256 nodal points ( $\Delta x = 1/256$ ), grid spacing in powers of two being suitable for spectral basis functions, ensuring grid-independence of the results. While exploring self-similarity, the grid size and time step values are further refined. We set  $\Delta x = 1/4096$  and use adaptive time stepping with lower end values of the order  $\Delta t \sim O(10^{-6})$ . We assume the film to have ruptured when the minimum height of the film  $h_{\min} \leq 10^{-4}$ .

### B. The “dilute limit”

#### 1. Evolution and parametric studies

The nonlinear dynamics using the LVM (14) for surface viscosity in a film with the dilute concentration of surfactants are discussed first. We remind that this is a special limit of the NVM as discussed in Sec. II B. Figure 5 shows spatiotemporal evolution profiles for the film height  $h$ , concentration  $\Gamma$ , and velocity at the interface  $c$  for a typical case. The profiles are plotted on spatial coordinates over a domain length  $\lambda$ . Given that the boundary conditions are periodic, successive crests/troughs in the profiles are separated by  $\lambda$ , consistent with expectations of the spinodal dewetting mechanism. The numerically obtained growth rate is also validated with the predictions of linear theory, as is shown in Fig. 5(a) (lower panel). At short times, the linear theory predictions are in agreement with the nonlinear solutions but deviate at later times closer to rupture, when the nonlinear terms become significant.

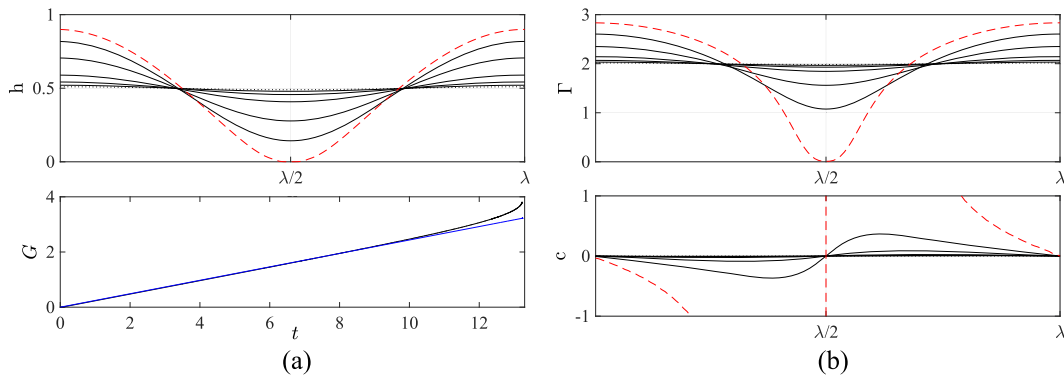


**FIG. 5.** Spatiotemporal evolution of the interface height [(a)-upper panel], surfactant concentration [(b)-upper panel], and tangential velocity [(b)-lower panel] for the linear model obtained by solving Eqs. (26)–(28) at various times  $t = 0, 3, 6, 9, 12, 13, 13.22$ . The initial condition at  $t = 0$  is shown by a dotted curve, and the rupture profile shown by the dashed curve occurs at  $t = 13.22$ . The other parameters used are  $D^{-1} = 50$ ,  $M = 10^{-3} = \beta$ ,  $B = 1$ ,  $Pe = 20$ ,  $Re = 2$ , and  $\Gamma_i^{(l)} = 2$ . [(a)-lower panel] Comparison of the numerically obtained growth rate and linear theory predictions. We define a nonlinear metric  $G = \log(\Delta h(t)/\Delta h(0))$ , where  $\Delta h(t)$  is the difference between the maximum and minimum values of  $h(x, t)$  at any time  $t$  (see Ref. 42).

Parametric studies on film evolution in the “dilute” regime reveal that qualitative features of evolution follow the trends observed in earlier studies.<sup>14,20</sup> The rapid formation of sharp ruptures in the profiles of  $h$  and  $\Gamma$  indicates the possibility of self-similar solutions close to rupture. Figure 6 shows the effect of surface viscosity ( $B$ ) and its linear concentration dependence (represented by  $\beta$ ) on the interface profile and film evolution kinetics. For smaller values of  $B$ , the surface viscosity contribution is lesser, and a sharp, pointed rupture is observed<sup>14,16</sup> as shown in Fig. 6(a) (top panel). Increasing  $B$  flattens the cusps formed in the vicinity of rupture. Surface viscosity may be interpreted as a diffusivity of surface velocity

or momentum; hence, it neutralizes velocity gradients at the surface. Therefore, there is greater advection of the liquid onto either side near the rupture location, resulting in a flatter rupture profile. On the other hand, increasing the parameter  $\beta$  produces a more cusp-like rupture, as shown in Fig. 6(b) (top panel). This is understandable since surface viscosity from (14) at the rupture location reduces to  $\eta|_{x=x_r} \approx 1 - \beta$  since  $\Gamma \ll 1$  near rupture. Therefore, increasing  $\beta$  reduces the local value of surface viscosity near the rupture location. It has to be noted that the maximum value of  $\beta$  cannot exceed unity as a result of positivity of  $\eta$ . The upper limit of  $\beta = 1$  causes the non-dimensional surface viscosity to become identical to the

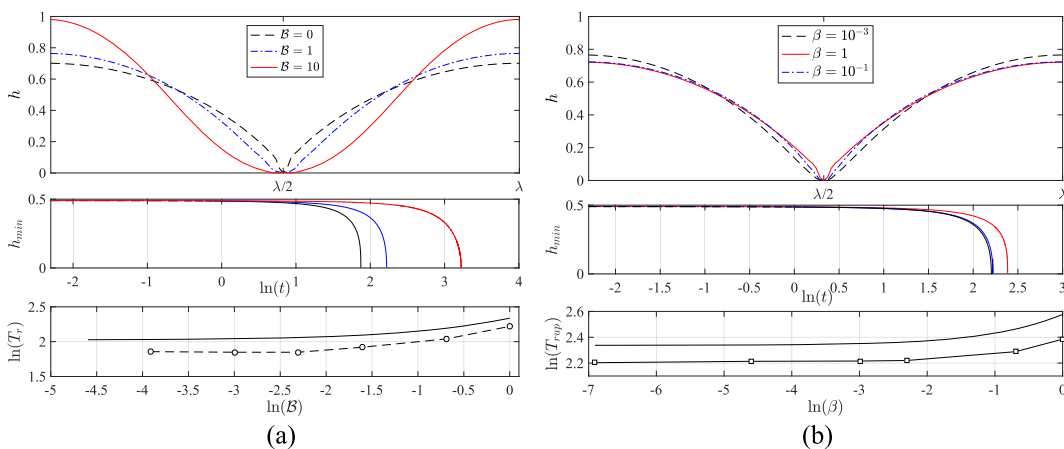


**FIG. 6.** Nonlinear results from the LVM obtained by solving (26)–(28). (a) Effect of the varying  $B$  on height profiles at the time of rupture with fixed  $\beta = 10^{-3}$ .  $B = 0$  corresponds to the case of zero surface viscosity and exhibits a cusp-like solution. (Lower panels) Evolution of the minimum film thickness ( $h_{min}$ ) with time and comparison of rupture time predictions from linear stability analysis (solid) and nonlinear simulations (circles) for the varying  $B$  as used in (a). (b) Effect of the varying  $\beta$  on height profiles at the time of rupture with  $B = 1$ . As  $\beta$  increases, the film profile near rupture approaches a cusp-like solution. (Lower panels) Evolution of the minimum film thickness ( $h_{min}$ ) with time and comparison of rupture time predictions from linear stability analysis (solid) and nonlinear simulations (squares) for the varying  $\beta$ . Other parameter values are fixed as  $D = 10^{-2}$ ,  $Pe = 1$ ,  $Re = 10^{-2}$ ,  $M = 10^{-3}$ , and  $\Gamma_i^{(l)} = 2$ .

non-dimensional surfactant concentration, i.e.,  $\eta|_{\beta=1} = \Gamma$ . Since  $\Gamma \rightarrow 0$  at the rupture location,  $\eta$  too vanishes at the rupture location. This causes the film profile to bear resemblance to that of a zero surface viscosity case as is clearly evident from the cusp-like profile at  $\beta = 1$  in Fig. 6(b). This profile matches very well with the case of zero surface viscosity,  $\mathcal{B} = 0$ , as shown in Fig. 6(a). This is further discussed in Sec. IV B 2. The rupture times appear to be of the same order of magnitude for a wide range of values of  $\beta$  as seen in Fig. 6(b) (lower panel).

## 2. Self-similar solutions

Next, we investigate the presence of self-similar behavior in free film profiles in the vicinity of the rupture location for the linear viscosity model. We assume solutions for the unknowns  $h(x, t)$ ,  $\Gamma(x, t)$ , and  $c(x, t)$  in the form

$$\begin{aligned} h(x, t) &= \tau^i H(\chi), & c(x, t) &= \tau^k U(\chi), \\ \Gamma(x, t) &= \tau^l G(\chi), & \chi(x, t) &= (x - x_r)/\tau^j, \end{aligned} \quad (52)$$

where  $\chi$  is the similarity variable and  $\tau = t_r - t$ ,  $x_r$  and  $t_r$  being the spatial location and time of rupture, respectively. Using  $\eta = 1 + \beta(\Gamma - 1)$  and substituting (52) into (26)–(28) give us the similarity equations, not shown here for brevity of this paper. To obtain scalings followed by  $h$ ,  $\Gamma$ , and  $c$ , we follow the approach used by Matar<sup>20</sup> and Vaynblat *et al.*<sup>15</sup> These scalings allow us to extract the exponents  $i, j, k, l$  without knowledge of rupture time *a priori*. Following their procedure, it is found that the scalings are unchanged for  $0 \leq \beta < 1$  and are found to be  $i = l = 1/2$ ,  $j = 1/4$ ,  $k = -3/4$ . These are the same scalings reported by Matar<sup>20</sup> and correspond to  $\beta = 0$  in our study. For the special case of  $\beta = 1$ , surface viscosity all along the interface reduces to the expression  $\eta \sim \Gamma$ . Since surfactant concentration at the rupture location becomes vanishingly small, surface viscosity too becomes negligible in the vicinity of rupture when  $\beta = 1$ . The following exponents are found for this case:  $i = l = 1/3$ ,  $j = 1/2$ ,  $k = -1/2$ , which is identical to the case with zero surface viscosity as obtained in Ref. 15 and corresponds to the case  $\mathcal{B} = 0$  within our study. There are two major points to be noted in the case of  $\beta = 1$ : (i) surface viscosity has a finite value away from the rupture point, and this leads to deviation of the interface shape from that reported in Ref. 15 in the far-field; (ii) this behavior is not seen for  $Pe \ll 1$  as surfactants are expected to be non-vanishing at the rupture location due to strong diffusion of the concentration field. Figure 7(a) shows the self-similar profiles at rupture for  $\beta = 0$  and  $\beta = 0.5$ .

The effect of the newly introduced variable in this study,  $\beta$ , is felt on the local film profile at the rupture location. As also observed in Fig. 6(b), as we increase the sensitivity of surface viscosity to surfactant concentration,  $\beta$ , the smoothening effect of surface viscosity is reduced and a “cusp-like” solution is observed. The underlying reason behind this result is further illustrated by Fig. 7(b), which shows the temporal evolution of the surface viscosity at the rupture point for  $\beta = 0$  and  $\beta = 0.1$  (concentration-driven surface viscosity). Even though the surface viscosity starts with a higher value than the constant viscosity case, the effect decreases near the rupture point for  $\beta > 0$ . The interface develops toward a more cusp-like profile (closer to profiles for  $\mathcal{B} = 0$ ) decreasing the surface viscosity even below the constant surface viscosity case. An even clearer picture can be seen

while examining the second derivative of the film profile as shown in Figs. 7(c) and 7(d).  $H_{\chi\chi}$ , which is a direct measure of the local curvature and clearly increases for  $0 < \beta < 1$ , reaching the maximum at  $\beta = 1$  (red), which is very close to the equivalent case of  $\mathcal{B} = 0$  (black). The curvature is seen to diverge as the interface moves toward rupture [see Fig. 7(d)] confirming a “cusp-like” behavior. For cases with non-zero surface viscosity at the rupture location, such a singularity is arrested, and the interface is flattened as seen in Fig. 7(d) for a specific case of  $\beta = 0.5$ . In other words, for the extreme case of  $\beta = 1$ , surface viscosity effects are suppressed completely at the rupture point and a cusp-like profile of a clean interface  $\Gamma = 0$  (or that of a particle-laden interface with no surface viscosity,  $\mathcal{B} = 0$ ) is recovered. Mathematically speaking, this implies that we can obtain a cusp-like profile for  $\beta = 1$ , however large the initial surface viscosity is chosen to be. Self-similarity is not seen in simulations with the NVM in the jammed limit due to the nonlinear nature of the model.

The scaling exponents discussed above also reveal the dominant balance of forces in the vicinity of rupture. This can be determined by substituting the exponents into the similarity equations for various cases. With  $\beta = 1$  and  $\mathcal{B} = 0$  (no surface viscosity), the dominant balance is between inertial, van der Waals, and viscous forces and the interface forms a cusp near rupture. In the case of  $0 \leq \beta < 1$ , the dominant balance is between inertial, van der Waals, and surface viscous forces. Viscous forces become sub-dominant as one approaches the rupture point. In all the above cases, capillary and Marangoni forces play a negligible role near rupture, consistent with observations in earlier studies.<sup>15,20</sup> The above dominant balance was further verified by comparing the magnitude of each term in the evolution equation (28).

In Sec. IV C, we investigate nonlinear evolution of the interface at high concentrations using the NVM for surface viscosity.

## C. The “jamming limit”

The rigidification of the interface in the limit of jammed state concentration of surfactants is arguably the most significant aspect of this work. The notion that films at the jamming limit are very stable as suggested by linear stability analysis can be visualized better through nonlinear simulations using the nonlinear viscosity model (NVM) for surface viscosity given by (15). Note that even though the surface viscosity can be effectively increased in the linear/constant model as well by choosing high values of  $\mathcal{B}$ , the NVM appears to be better suited to realistic conditions where surface concentration evolves dynamically. Viscosity in the NVM diverges to a very high value with the change in the local concentration rendering part of the interface immobile as will be shown below.

First, the NVM is validated in the limit of dilute concentrations with results obtained from the LVM. To do so, the values of  $\alpha$ ,  $\beta$ ,  $\tilde{\Gamma}_{\text{dil}}$ , and  $\tilde{\Gamma}_{\text{max}}$  are chosen so as to satisfy the relation (16). Film profiles are plotted in the limit of weak concentration ( $\Gamma_i^{(l)} = 2.1$ ,  $\beta = 0.1$  in the linear model,  $\Gamma_i^{(nl)} = 0.1$ ,  $\alpha = 2$  in the NVM). This is illustrated in Fig. 10(b) in Appendix B, and both the film profiles seem to be in agreement in this limit. Next, we study the effect of high surfactant concentration for which the NVM is ideally suited. The height profile and the surfactant concentration profile for the

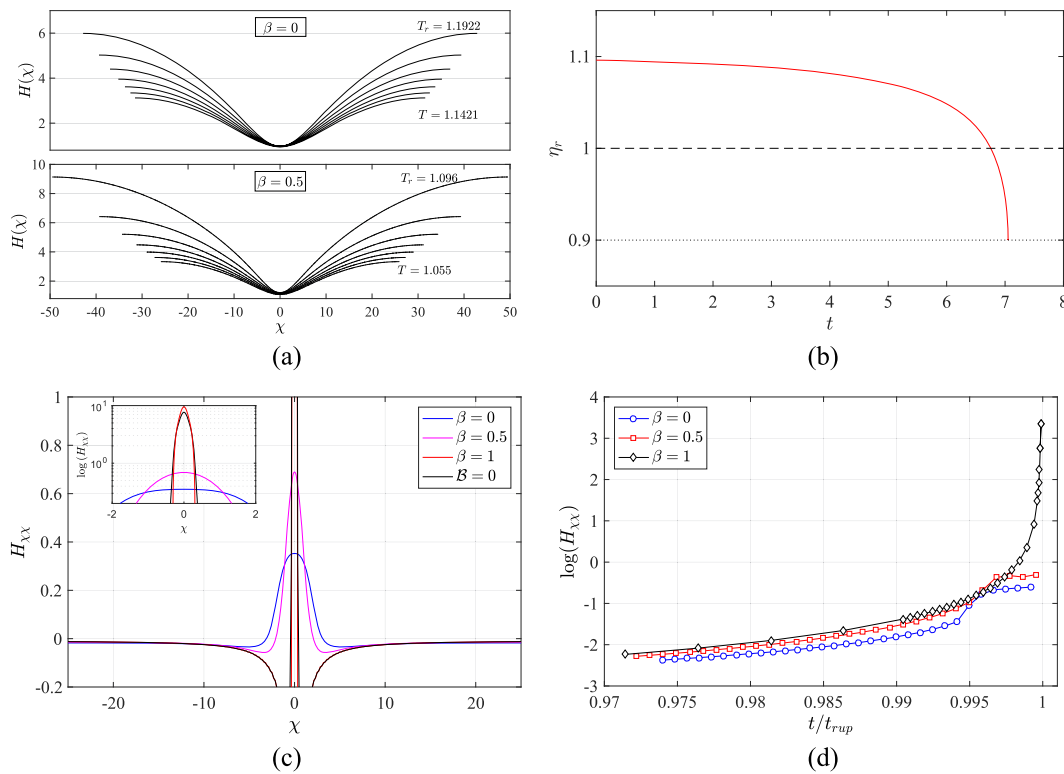


**FIG. 7.** Results from self-similarity analysis. (a) Self-similar film profiles at the rupture location close to the breakup time  $T_r = 1.192$  for  $\beta = 0$  and  $T_r = 1.096$  for  $\beta = 0.5$ . (b) Variation of surface viscosity with time at the rupture location for the linear model with  $\beta = 0.1$  (solid) and constant surface viscosity (dashed),  $\beta = 0$ . The value of  $\eta_{ref}$  is also shown in the figure, and it denotes the value of reference surface viscosity on a clean interface. At the rupture location, the surfactant concentration goes to zero causing  $\eta$  to approach  $\eta_{ref}$ . Note that the surface viscosity at the rupture location for  $\beta = 0.1$  is lower than that for a case with constant surface viscosity,  $\beta = 0$ . (c) Curvature,  $H_{\chi\chi}$ , of the self-similar interface profile just before rupture time. The final profile for  $\beta = 0.5$  (pink) exhibits a larger curvature than that in the case of  $\beta = 0$  (blue) owing to lower surface viscosity as discussed in (b). (Inset) Zoomed in log-plots showing cusp-like behavior for a film devoid of surface viscosity,  $\mathcal{B} = 0$  (black). (d) Evolution of the curvature at the rupture location with time. A diverging curve with time confirms a “cusp-like” behavior. Other parameters are  $Pe = 1$ ,  $M = 10^{-1}$ ,  $Re = 10^{-2}$ ,  $\mathcal{D} = 10^{-3}$ ,  $\mathcal{B} = 1$ , and  $\Gamma_i^{(l)} = 2$ .

particular values  $\Gamma_i^{(nl)} = 0.8$  and  $\alpha = 2$  of the NVM are shown in Fig. 8(a). The film stiffens and tends to be immobile all along the interface except in a narrow region at the center of the domain where height and concentration profiles are at a minimum. Unlike in earlier cases, the film thinning occurs in a very narrow region. This evolution quickly deviates from the evolution in the LVM (not shown), which typically follows a smooth amplifying sinusoidal structure. The peculiar film shape obtained in the NVM is more elegantly demonstrated in the plots of the film height profile for different initial surfactant concentrations. Figure 8(b) compares film shapes at rupture for three different initial concentrations: a dilute limit at  $\Gamma_i^{(nl)} = 0.1$ , an intermediate regime at  $\Gamma_i^{(nl)} = 0.6$ , and a near-jammed state limit at  $\Gamma_i^{(nl)} = 0.9$ . The profiles in the dilute limit exhibit a large radius of curvature and are equivalent to the film profiles seen in Sec. IV B 1. In the near-jammed limit, the film thinning occurs over a very narrow region within the interface. It has to be noted that the interface flattens at the vicinity of rupture but nevertheless has a small non-vanishing radius of curvature. The

case of  $\Gamma_i^{(nl)} = 1$  is a singular limit and cannot be solved numerically. This is consistent with the perturbation solution carried out in Sec. III A.

A particularly interesting result is the evolution of tangential velocity,  $c(x, t)$ , on the interface with the varying concentration as shown in Fig. 8(c). It is clear that the maximum tangential velocity decreases and asymptotes toward zero with the increasing concentration, suggesting a transition from a mobile interface for  $\Gamma_i^{(nl)} = 0$  to an immobile interface at the jammed state. Such a surface viscosity-driven transition from partially mobile to immobile interfaces has also been reported by Danov *et al.*<sup>26</sup> For drainage of a thin liquid film between two gas bubbles, interfacial resistance arising from surface viscosity has been reported.<sup>40</sup> Consequently, the kinetics of film breakup is also found to slow down drastically with the increase in the concentration, and the rupture time diverges to infinity as  $\Gamma_i^{(nl)} \rightarrow 1$  as shown in Fig. 8(d). This is a key finding of the present study. This suggests that the interface behaves solid-like with very slow deformation near the

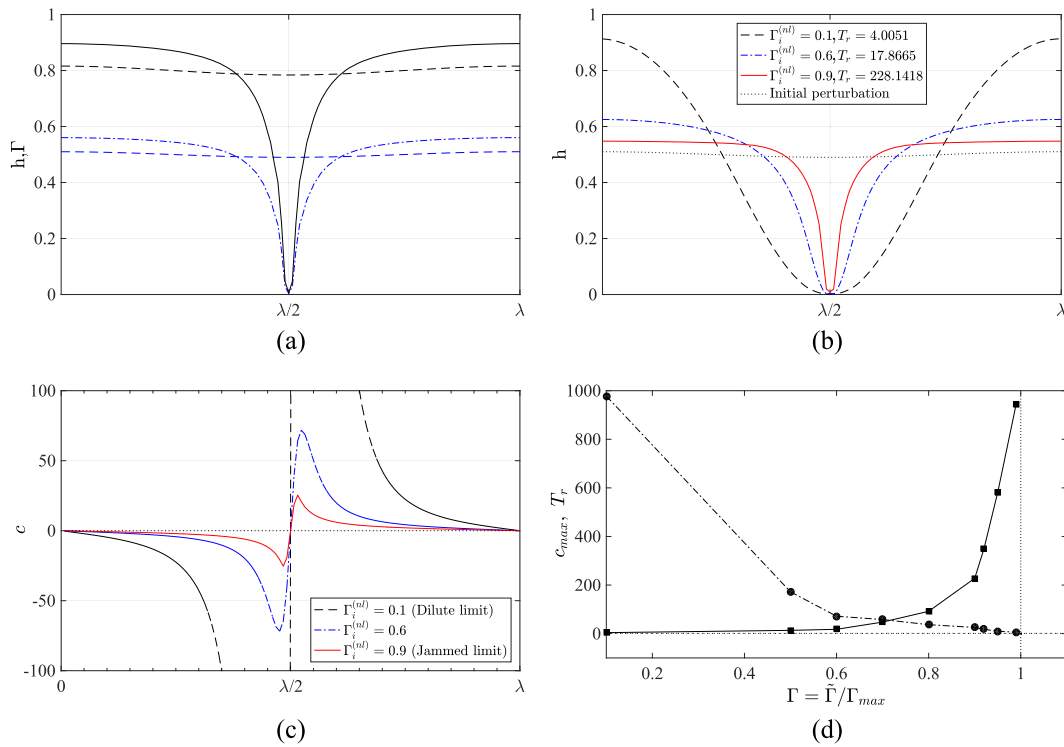


**FIG. 8.** Evolution of film profiles using the NVM obtained by solving Eqs. (26)–(28). (a) Height profiles (solid) and surfactant profile (dotted-dashed) at the instance of rupture for  $\Gamma_i^{(nl)} = 0.8$ . The dashed lines represent the initial perturbation. (b) Height profiles for three different values of surfactant concentration ranging from the dilute ( $\Gamma_i^{(nl)} = 0.1$ ), the intermediate ( $\Gamma_i^{(nl)} = 0.6$ ), to the jamming ( $\Gamma_i^{(nl)} = 0.9$ ) limit occurring at three different rupture times  $T_r = 4.051, 17.866, 227.843$ , respectively. The interface profile is remarkably different in the three cases, and so is the rupture time. (c) Corresponding tangential velocities at rupture,  $c(x, T_r)$ , for the varying  $\Gamma_i^{(nl)}$ , plotted just before rupture. (d) Maximum tangential velocity  $c_{max}$  (dotted-dashed) and rupture time  $T_r$  (solid) plotted for various values of  $\Gamma_i^{(nl)}$ . Other parameters are fixed as  $Pe = 1, \mathcal{D} = 10^{-3}, Re = 10^{-2}, M = 10^{-1}, \mathcal{B} = 1, \alpha = 2$ .

jamming limit. It has to be noted that rupture cannot be completely prevented to provide absolute stabilization of the interface. Surface viscosity can at most act as a retarding effect, but at very large times, van der Waals forces will eventually prevail causing rupture.

To distinguish between the linear and nonlinear viscosity models in the nonlinear evolution, we now briefly examine the rupture process using the two models. It is shown in Sec. III that only an effective viscosity,  $\eta_{eff}$ , enters the dispersion relation and the

exact nature of the viscosity model is unimportant. Hence, if the same base-state viscosity is used with both models, the growth rate obtained remains unchanged. Furthermore, the same growth rate is obtained for a constant viscosity case as studied by Matar.<sup>20</sup> We now show that despite the similarity in the linear regime, nonlinear evolution of the interface strongly depends on the functional form of the viscosity model employed. To illustrate this, we use a fixed value of non-dimensional surface viscosity for four different scenarios described in the following:

$$\eta_{eff} = \begin{cases} 62.5 & \text{for constant viscosity model} \\ \mathcal{B} \left[ 1 + \beta \left( \Gamma_i^{(l)} - 1 \right) \right] & \text{for LVM with } \mathcal{B} = 50, \beta = 0.25, \text{ and } \Gamma_i^{(l)} = 2 \\ \mathcal{B} \left[ 1 - \Gamma_i^{(nl)} \right]^{-\alpha} & \text{for NVM with } \mathcal{B} = 10, \alpha = 2, \text{ and } \Gamma_i^{(nl)} = 0.6 \\ \mathcal{B} \left[ 1 - \Gamma_i^{(nl)} \right]^{-\alpha} & \text{for NVM with } \mathcal{B} = 10, \alpha = 3, \text{ and } \Gamma_i^{(nl)} = 0.46. \end{cases} \quad (53)$$

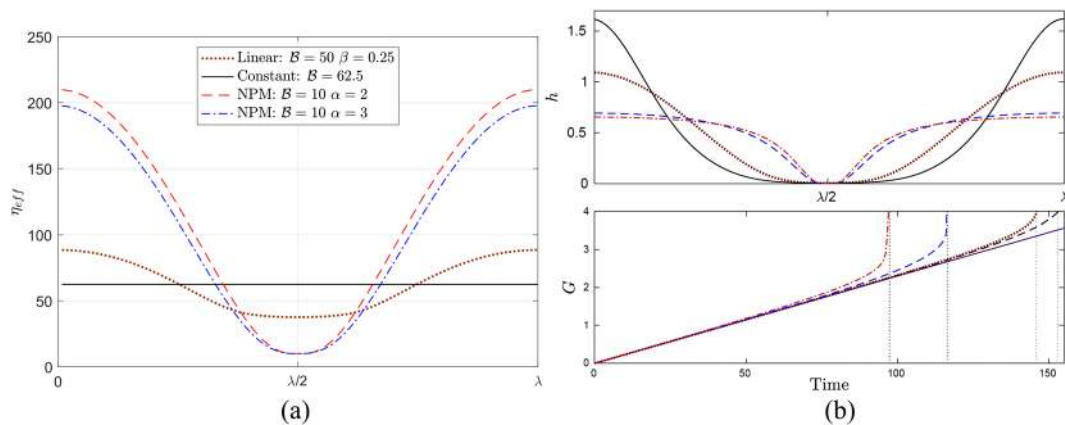


**FIG. 9.** Comparison of film profiles for various surface viscosity models with the same effective surface viscosity initially. (a) Surface viscosity evaluated just before rupture for various models. Note the linear model gives a higher surface viscosity at the rupture location than the nonlinear models. This leads to a higher rupture time than that in the nonlinear models as shown in (b). The film profiles at rupture are also distinct for the various models. Other parameters are fixed as  $Pe = 1$ ,  $D = 10^{-2}$ ,  $Re = 10^{-2}$ ,  $M = 0$ .

The above parameters are chosen arbitrarily only to illustrate the role played by surface viscosity models. Though all the four cases have the same value of initial base-state viscosity, interfacial viscosity at later times evolves according to the evolution of surface concentration and is shown in Fig. 9(a) at the time of rupture. For both LVM and NVM cases, since the concentration decreases near the rupture location, the effective viscosity is reduced in this region as is clearly evident in the plot. It has to be noted that the surface viscosity does not reduce to zero even if the concentration drops to zero near rupture. Furthermore, surface viscosity can assume very large values away from the rupture location, especially in the NVM cases, making the region practically immobile. The interface shapes close to rupture time for the four cases are shown in Fig. 9(b). Since the constant viscosity case has the highest value of surface viscosity at the rupture location, it also has the lowest curvature exhibiting pronounced flattening near the rupture point. Clearly, interface shapes are remarkably different in each case suggesting that the functional form of surface viscosity can play an important role. Since linear stability analysis only depends on the base value of the surface viscosity, all the four cases given in (53) have the same dominant growth rate. Yet, it is clearly evident in Fig. 9(b) that NVM cases exhibit the fastest rupture, while constant viscosity cases exhibit the slowest rupture. This is understandable since in the constant viscosity cases, resistance from surface viscosity is equal at all points on the interface, whereas in variable viscosity cases, a decrease in the concentration in certain regions reduces surface viscosity locally. This leads to rupture being favored in these locations. Given that the concentration is expected to change when the interface deforms, a variable surface viscosity model is more realistic than a constant viscosity model.

The above results also demonstrate how mobility along the interface varies with surface viscosity and how this can have an important influence on the dynamical evolution of interfaces. The results above perhaps show a simple way to model fluid–fluid systems with variable surface viscosity effects and provide a simple

recipe to describe a smooth transition from the free-slip regime to the no-slip regime such as in the case of a surfactant-laden sedimenting drop (see Ref. 27). Besides, they provide an elegant fluid dynamical explanation for enhanced stability of certain surfactant-stabilized emulsions and Pickering emulsions.

## V. SUMMARY AND DISCUSSIONS

We have formulated a unified model that includes various interfacial effects due to the presence of surface-active agents in a thin free film. Apart from intermolecular forces and Marangoni effects, it is shown that surface viscosity effects play a key role in determining the stability of a thin film. It is well known that Marangoni effects due to surfactant driven surface tension gradients stabilize a thin film, but this stabilization does not explain the long shelf-life of certain surfactant-stabilized emulsions and Pickering emulsions. Marangoni stabilization only tends to delay rupture marginally. We have shown that concentration-dependent surface viscosity mediated stabilization is a missing element in most earlier studies and offers a theoretical tool to analyze long shelf-life of such emulsions. As a canonical problem, stability of a free film is studied and the theory can be easily extended to bounded films and other interfacial problems. To better illustrate the dependence of surface viscosity on surfactant concentration, two distinct phenomenological models are employed. In the linear viscosity model (LVM), surface viscosity varies linearly with surfactant concentration and is expected to be suited to dilute limits. The nonlinear model allows us to probe the role of surface viscosity profile in greater detail. In the nonlinear viscosity model (NVM), surface viscosity varies nonlinearly with the concentration such that it diverges at a critical concentration, which is termed the “jamming limit.” The two models are shown to concur in the dilute limit, and this lends validity to the nonlinear model at all concentrations.

In the LVM, surface viscosity stabilizes the film with the increasing Boussinesq number but does not affect the cut-off

wavenumber. On the other hand, the NVM drastically alters the stability characteristics of the thin film. The growth rate is found to scale with  $\delta = (1 - \Gamma_i^{(nl)})^\alpha$ , where  $0 < \Gamma_i^{(nl)} < 1$  is the non-dimensional concentration scaled in terms of the “jamming limit” concentration,  $\Gamma_{\max}$ . The parameter  $\delta$  can thus be made arbitrarily small near the jamming limit. This leads to a dramatic stabilization of the thin film and significantly delays rupture in the nonlinear simulations. Using standard perturbation techniques, analysis of the dispersion relation yields a simple criterion for enhanced film stability. It is found that when  $\Gamma_i^{(nl)} > 3\mathcal{D}/M$ , stability of the thin film is dramatically enhanced. This suggests that surfactant concentration can be arbitrarily increased beyond a critical value ( $= 3\mathcal{D}/M$ ) to achieve enhanced stabilization of the film. However, in reality, such concentrations are difficult to achieve for realistic parameter values of  $M$  and  $\mathcal{D}$ . A key finding of the present paper is that rupture times can be arbitrarily increased by tuning the surfactant concentration. This stabilization is achieved via surface viscosity effects, which increase nonlinearly with surfactant concentration in the jamming limit. Large surface viscosities render the interface immobile, which helps counteract the rupture process by slowing down film evolution.

The findings of this work have relevance to many other experimental and theoretical works. Experiments with rising drops/sedimenting bubbles have revealed that surfactants enhance the drag force on the drop/bubble.<sup>27</sup> This effect has been modeled theoretically using a spherical cap approximation<sup>27,28</sup> wherein surfactants are assumed to be in a jammed state on the leeward side of the drop/bubble and are assumed to be absent on the rest of the surface. A no-slip condition is employed on the spherical cap and a stress-free condition on the rest of the surface. The NVM employed here leads to a smooth transition from the no-slip to the stress-free condition on the interface and prevents a jump in the interface conditions as was seen by Sadhal and Johnson.<sup>28</sup> Our results are also consistent with those in Ref. 26 in which the interface mobility was found to reduce with the increasing surfactant concentration. This has direct significance to the stability of Pickering emulsions.<sup>43,44</sup> There is sufficient anecdotal evidence in the literature on Pickering emulsions<sup>2</sup> that shows that removing adsorbed particles (by changing the pH of the aqueous phase) reduces emulsion stability dramatically. The treatment of the surface-active agents as “surfactants” also allows one to look at proteins in food systems as surface-active agents.<sup>45</sup> A few studies have found that truly stable foams can only be formed when coagulated proteins form a rigid solid network on the interface,<sup>46,47</sup> although much more complex forces come into play in this scenario.

A number of interesting features remain unexplored. Though nonlinear surface viscosity effects successfully explain the transition from mobile to immobile interfaces, they do not account for elasticity found in particle-laden interfaces. Liquid marbles<sup>48</sup> and particle-coated bubbles can sustain non-spherical shapes upon compression.<sup>49</sup> This could be due to anisotropic surface tension or elasticity or both. Studies with particle-covered Landau–Levich dip-coating flows<sup>50</sup> reveal that elastic effects play an important role in explaining experimental power-law dependence between coating thickness and withdrawal speed. It is therefore imperative that future studies incorporate a combination of variable surface viscosity and elasticity to better predict characteristics of

particle/surfactant-covered interfacial systems, especially when jamming is expected to occur.

### AUTHORS' CONTRIBUTIONS

H.N.D. and S.K.K. defined the scope and supervised this study, V.K.P. carried out the initial mathematical modeling, and A.C. carried out subsequent analytical and numerical calculations in this study. H.N.D., S.K.K., and A.C. analyzed the results and wrote the manuscript.

### ACKNOWLEDGMENTS

An earlier version of this work was presented by one of the authors (A.C.) at AIChE Annual Meeting 2018, and A.C. thanks Dr. Ashutosh Ricchariya (LVPEI, Hyderabad) and Department of Biotechnology, Govt. of India, for travel support. H.N.D. and S.K.K. thank Pavan Pujar from NIT Surathkal who carried out preliminary analysis of this work. The authors gratefully acknowledge Professor James J. Feng (UBC, Vancouver) and Dr. K. Badarinath (IIT Hyderabad) for their critical reading of the manuscript and constructive suggestions. A.C. was supported by a doctoral fellowship from the Ministry of Human Resource Development, Govt. of India, and H.N.D. thanks partial support from an Early Career Research Award (Grant No. ECR/2015/000086).

## APPENDIX A: INTERFACIAL BOUNDARY CONDITIONS AND x-MOMENTUM EQUATION

### 1. Normal stress balance

For a 1D interface, the normal stress balance assumes the form

$$-\bar{n} \cdot \|T\| \cdot \bar{n} = 2\kappa\sigma + 2\kappa(k^s + \mu^s)\bar{\nabla}_s \cdot \bar{u}. \quad (A1)$$

We resolve the  $\bar{\nabla}_s$  curvilinear gradient operator and the tensor products to get a PDE in Cartesian coordinates. This is done analytically and validated using the technical computing software *Mathematica*. The dimensional equation turns out to be

$$-\bar{P} + \frac{1}{(1 + \tilde{h}_x^2)^{5/2}} [-\tilde{\sigma}(1 + \tilde{h}_x^2)\tilde{h}_{xx} - \mu\{\mathbb{A}\}\{\mathbb{B}\}] = 0, \quad (A2)$$

where

$$\begin{aligned} \mathbb{A} &= 2\sqrt{1 + \tilde{h}_x^2} + 2\tilde{h}_x^2\sqrt{1 + \tilde{h}_x^2} + \frac{\tilde{\eta}}{\mu}\tilde{h}_{xx}, \\ \mathbb{B} &= -\tilde{v}_z + \tilde{h}_x\{\tilde{u}_z + \tilde{h}_x(\tilde{v}_z + \tilde{v}_{xx})\}. \end{aligned}$$

Here, the surface dilatational ( $k^s$ ) and surface shear ( $\mu^s$ ) viscosities are combined into a parameter  $\eta$ , since they occur in additive pairs in the equations. This is only observed for a 1D interface. Inserting relevant scalings (9)–(13) as discussed in the main text, we observe the pressure term appears at leading order followed by the capillary term at  $O(\epsilon)$ . Hence, the disjoining pressure number ( $\mathcal{D}^{-1}$ ) (or  $\sigma$ ) is rescaled to retain capillary effects. We obtain the final simplified



non-dimensional PDE, which reads

$$-P + \left[ -\mathcal{D}^{-1}h_{xx} - \epsilon^2\mathcal{D}^{-1}M(\Gamma - 1) - \left\{ 2(1 + \epsilon^2h_x^2) + \epsilon^2\mathbb{B}\frac{\eta}{h_{xx}} \right\} \right. \\ \left. \times \{-v_z + h_xu_z + \epsilon^2h_x^2v_z + \epsilon^3h_x^2v_x\} \right] = 0. \quad (\text{A3})$$

Considering only the leading order terms, we get (23) used in deriving the film evolution equations.

## 2. Tangential stress balance

For a 1D interface, the tangential stress balance assumes the form

$$-\bar{t} \cdot \|T\| \cdot \bar{n} = \bar{t} \cdot \bar{\nabla}_s \sigma + (k^s + \mu^s)\bar{t} \cdot \bar{\nabla}_s \bar{\nabla}_s \cdot \bar{u} \\ + \bar{t} \cdot \bar{\nabla}_s (k^s + \mu^s)\bar{\nabla}_s \cdot \bar{u}. \quad (\text{A4})$$

The dimensional equation turns out to be

$$\bar{\sigma}_{\bar{x}}(1 + \bar{h}_{\bar{x}}^2)^2 + \mu\sqrt{1 + \bar{h}_{\bar{x}}^2}[-\bar{u}_{\bar{z}} + \bar{h}_{\bar{x}}^4\bar{u}_{\bar{z}} - 4\bar{h}_{\bar{x}}\bar{v}_{\bar{z}}(1 + \bar{h}_{\bar{x}}^2) + \bar{v}_{\bar{z}}(\bar{h}_{\bar{x}}^4 - 1)] \\ + \bar{\eta}_{\bar{x}}(1 + \bar{h}_{\bar{x}}^2)[- \bar{v}_{\bar{z}} + \bar{h}_{\bar{x}}(\bar{u}_{\bar{z}} + \bar{h}_{\bar{x}}\bar{v}_{\bar{z}} + \bar{v}_{\bar{x}})] \\ + \bar{\eta}[\bar{h}_{\bar{x}}^3\bar{v}_{\bar{z}\bar{z}} + \bar{h}_{\bar{x}}(\bar{u}_{\bar{z}\bar{z}} + \bar{v}_{\bar{x}}) + \bar{h}_{\bar{x}}^2(\bar{u}_{\bar{z}\bar{z}} - \bar{h}_{\bar{x}\bar{x}}(\bar{u}_{\bar{z}} + \bar{v}_{\bar{x}}) + \bar{v}_{\bar{x}\bar{z}}) \\ - \bar{v}_{\bar{x}\bar{z}} + \bar{h}_{\bar{x}}^4(\bar{u}_{\bar{z}\bar{z}} + 2\bar{v}_{\bar{x}\bar{z}}) + \bar{h}_{\bar{x}}^3(\bar{u}_{\bar{x}\bar{z}} + \bar{v}_{\bar{x}\bar{x}}) \\ + \bar{h}_{\bar{x}}(4\bar{h}_{\bar{x}\bar{x}}\bar{v}_{\bar{z}} - \bar{v}_{\bar{z}\bar{z}}) + \bar{u}_{\bar{x}\bar{z}} + \bar{v}_{\bar{x}\bar{x}}] = 0. \quad (\text{A5})$$

Inserting relevant scalings and simplifying, we obtain the final non-dimensional PDE

$$\mathcal{D}^{-1}\sigma_x - u_z + (\epsilon h_x)^4 u_z - 4\epsilon^2 h_x v_z (1 + (\epsilon h_x)^2) - \epsilon^2 v_x + \epsilon^6 h_x^4 v_x \\ + \epsilon^2 \mathcal{B}\eta_x (-v_z + h_x u_z + \epsilon^2 h_x v_z + \epsilon^2 v_x) + \epsilon^2 \mathcal{B}\eta (\epsilon^4 h_x^5 + h_{xx} u_z \\ + \epsilon^2 h_{xx} v_x - v_{xz} - \epsilon^2 h_{xx} h_x^2 u_z - \epsilon^4 h_{xx} h_x^2 v_x + \epsilon^2 h_x^2 v_{xz} (1 + \epsilon^2 h_x^2) \\ + h_x^2 u_{zz} (1 + \epsilon^2 h_x^2) + h_x u_{xz} (1 + \epsilon^2 h_x^2) + \epsilon^2 h_x v_{xx} (1 + \epsilon^2 h_x^2) \\ + 4\epsilon^2 h_x h_{xx} v_z - h_x v_{zz}) = 0. \quad (\text{A6})$$

The above equation reduces to (25) when the leading order terms are considered. The first order corrections of this equation used to

derive (28) can also be realized when  $O(\epsilon^2)$  terms are considered. As can be observed clearly, the surface viscosity enters the equations in the first order corrections of the tangential stress boundary condition and has highly nonlinear coupling with the height and various velocity gradient terms.

## 3. x-Momentum equation

The non-dimensional x-momentum equation valid to  $O(\epsilon^2)$  takes the form

$$u_{zz} = \epsilon^2 \text{Re}(u_t + uu_x + vu_z) + \epsilon^2 (P + \phi)_x - \epsilon^2 u_{xx}. \quad (\text{A7})$$

Expanding all terms in powers of  $\epsilon^2$ , the leading order equation becomes

$$u_{zz}^{(0)} = 0, \quad (\text{A8})$$

and the first order equation at  $O(\epsilon^2)$  assumes the form

$$u_{zz}^{(1)} = \epsilon^2 \text{Re}(u_t^{(0)} + u^{(0)}u_x^{(0)} + v^{(0)}u_z^{(0)}) + \epsilon^2 (P^{(0)} + \phi^{(0)})_x - \epsilon^2 u_{xx}^{(0)}, \quad (\text{A9})$$

where superscripts 0 and 1 denote leading and first order correction terms, respectively, in the asymptotic expansion (1). Integrating (A9) and using the symmetry boundary condition at  $z = 0$  [see Eq. (8)], we obtain an expression for  $u_z^{(1)}$ , which when compared to the first order correction of (A6) gives the third nonlinear evolution equation (28).

## APPENDIX B: NOTES ON THE VALIDITY OF SCALINGS FOR $\bar{\eta}_s$

A graphical illustration of the LVM and NVM is shown in Fig. 10(a). The LVM adds small corrections to the surface viscosity to exhibit weak relationship with surfactant concentration. We may consider it to be apt in two situations: (i) when the system

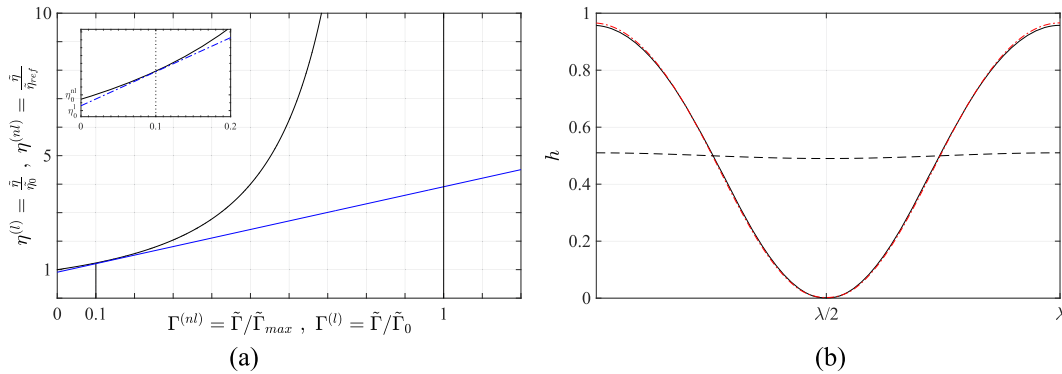


**FIG. 10.** (a) Graphical illustration of linear and nonlinear surface viscosity models given in Eqs. (14) and (15). The dilute limit of the nonlinear viscosity model (NVM) approaches the LVM as shown in the figure. This comparison serves to define a suitable “dilute” limit of the NVM in order to compare growth rate and film evolution curves for the two models. For the specific case of  $\beta = 10^{-3}$  and  $\alpha = 2$ , the two models have the same “effective” non-dimensional surface viscosity for  $\Gamma_i^{(nl)} = 0.1$ . (Inset) Zoomed in version for  $\Gamma^{(nl)} = 0-0.2$  (dilute limit).  $S = (\beta + \alpha)/\beta$  is the normalization constant. (b) Comparison of the height profile at rupture between the LVM and the NVM in the dilute limit. For the LVM,  $\Gamma_i^{(l)} = 2.1, \beta = 0.1, T_r = 3.588$ . For the NVM,  $\Gamma_i^{(nl)} = 0.1, \alpha = 2, T_r = 3.613$ . Other parameters are fixed as  $Pe = 1, \mathcal{D} = 10^{-3}, Re = 10^{-2}, M = 10^{-1}, \mathcal{B} = 1$ .

demands to have a linear relationship such as in polymer blends and (ii) when the surfactants are sparsely distributed on the interface (dilute limit). We focus on case (ii) in this work to validate it with the NVM defining surface viscosity as

$$\begin{aligned} \tilde{\eta}^{(l)} &= \tilde{\eta}_{\text{ref}}|_{\tilde{\Gamma}=\tilde{\Gamma}_{\text{dil}}} + \frac{\partial \tilde{\eta}}{\partial \tilde{\Gamma}}|_{\tilde{\Gamma}=\tilde{\Gamma}_{\text{dil}}} (\tilde{\Gamma} - \tilde{\Gamma}_{\text{dil}}) \\ \Rightarrow \tilde{\eta}^{(l)} &= \tilde{\eta}_{\text{dil}} \left[ 1 + \beta \left( \frac{\tilde{\Gamma} - \tilde{\Gamma}_{\text{dil}}}{\tilde{\Gamma}_{\text{dil}}} \right) \right], \end{aligned} \quad (\text{B1})$$

where  $\tilde{\eta}_0$  is the surface viscosity at a surfactant concentration within the dilute limit  $\tilde{\Gamma} = \tilde{\Gamma}_0$ . The definition of  $\beta$  as given in Table II can also be realized in the above equation. The surface viscosity for the NVM is defined as

$$\tilde{\eta}^{(nl)} = \tilde{\eta}_{\text{ref}}|_{\tilde{\Gamma}=0} \left( 1 - \frac{\tilde{\Gamma}}{\tilde{\Gamma}_{\text{max}}} \right)^{-\alpha}, \quad (\text{B2})$$

which diverges at  $\tilde{\Gamma} \rightarrow \tilde{\Gamma}_{\text{max}}$ . We can linearize this model for any arbitrary surfactant concentration and compare it to the linear model to obtain an equivalence relation

$$\frac{\tilde{\Gamma}_{\text{dil}}}{\tilde{\Gamma}_{\text{max}}} = \frac{\beta}{\beta + \alpha}. \quad (\text{B3})$$

Since  $\beta$  cannot exceed 1, we also have an additional constraint

$$\tilde{\Gamma}_{\text{dil}} \leq \frac{\tilde{\Gamma}_{\text{max}}}{\alpha + 1}. \quad (\text{B4})$$

Note the advantage of defining the linear model for an arbitrary  $\tilde{\Gamma}_{\text{dil}}$  and not for  $\tilde{\Gamma}_{\text{ref}} = 0$  (clean interface). This definition renders the linear model valid about any value of reference surfactant concentration  $\tilde{\Gamma}_{\text{ref}}$  when  $\beta$  at that concentration is known.

Having established the criterion for comparing the linear and nonlinear models in the dilute limit, we show that this comparison is robust and yields identical film profiles even in the nonlinear regime as shown in Fig. 10(b), which shows the comparison of height profiles from the two models at the instance of rupture.

### APPENDIX C: ON THE “WEAK MARANGONI” AND “WEAK SURFACE VISCOSITY” LIMITS

Equation (17) has been referred to as the leading order version of (13) in the “weak Marangoni” limit. The idea may be explained as follows. If terms of  $O(\epsilon^2)$ ,  $O(\epsilon^4)$ , etc., in (A6) are ignored and only leading order terms are retained, one arrives at

$$\mathcal{D}^{-1} \sigma_x - u_z = 0. \quad (\text{C1})$$

Substituting (13) into (C1) would yield

$$-\mathcal{D}^{-1} M \Gamma_x - u_z = 0, \quad (\text{C2})$$

which would imply that Marangoni effects are retained at leading order in the tangential stress balance condition. However, if one assumes that  $M$  itself is of  $O(\epsilon^2)$ , then the first term in (C2) would be neglected, with the simplified condition  $u_z^{(0)} = 0$ , as shown in Sec. II C. We term this the “weak Marangoni” limit, which is accomplished by setting  $M = \epsilon^2 \hat{M}$ , where  $\hat{M}$  is an  $O(1)$  parameter. This is also the limit explored previously by De Wit *et al.*<sup>16</sup> and Matar.<sup>20</sup> However, Marangoni effects would indeed be present at first order,

if one considers the  $O(\epsilon^2)$  corrections to the tangential stress balance (A6). A model that retains  $M$  as an  $O(1)$  parameter in (C2) may be termed the “strong Marangoni” limit and has been examined by Hwang *et al.*,<sup>51</sup> though in the absence of surface viscosity.

With reference to surface viscosity, it is evident from (A6) and its accompanying discussion that  $\eta$  drops out of the leading order tangential stress balance, i.e., when terms of  $O(\epsilon^2)$  or smaller are ignored. Hence, the formulation in the present work may be termed the “weak surface viscosity” regime. The analogous “strong surface viscosity” regime may be pursued through the rescaling  $\eta = \epsilon^{-2} \hat{\eta}$ , with  $\hat{\eta}$  being the new  $O(1)$  parameter, so that surface viscosity appears at leading order in (A6).

### DATA AVAILABILITY

The data that support the findings of this study are available from the corresponding author upon reasonable request.

### REFERENCES

- <sup>1</sup>T. F. Tadros, *Formulation of Disperse Systems* (Wiley-VCH, Weinheim, Germany, 2014).
- <sup>2</sup>T. G. Anjali and M. G. Basavaraj, “Influence of pH and salt concentration on Pickering emulsions stabilized by colloidal peanuts,” *Langmuir* **34**, 13312–13321 (2018).
- <sup>3</sup>L. Ye, H. You, J. Yao, and H. Su, “Water treatment technologies for perchlorate: A review,” *Desalination* **298**, 1–12 (2012).
- <sup>4</sup>X. Mao, R. Jiang, W. Xiao, and J. Yu, “Use of surfactants for the remediation of contaminated soils: A review,” *J. Hazard. Mater.* **285**, 419–435 (2015).
- <sup>5</sup>W. Ramsden, “Separation of solids in the surface-layers of solutions and ‘suspensions,’” *Proc. R. Soc. London* **72**(477-486), 156–164 (1904).
- <sup>6</sup>S. U. Pickering, “CXCVI.—Emulsions,” *J. Chem. Soc., Trans.* **91**, 2001–2021 (1907).
- <sup>7</sup>P. G. de Gennes, ““Young” soap films,” *Langmuir* **17**, 2416–2419 (2001).
- <sup>8</sup>S. Naire, R. J. Braun, and S. A. Snow, “An insoluble surfactant model for a vertical draining free film,” *J. Colloid Interface Sci.* **230**, 91–106 (2000).
- <sup>9</sup>S. Naire, R. J. Braun, and S. A. Snow, “An insoluble surfactant model for a vertical draining free film with variable surface viscosity,” *Phys. Fluids* **13**(9), 2492–2502 (2001).
- <sup>10</sup>R. J. Braun, S. Naire, and S. A. Snow, “Limiting cases of gravitational drainage of a vertical free film for evaluating surfactants,” *SIAM J. Appl. Math.* **61**(3), 889–913 (2000).
- <sup>11</sup>M. Prévost and D. Gallez, “Nonlinear rupture of thin free liquid films,” *J. Chem. Phys.* **84**(7), 4043–4048 (1986).
- <sup>12</sup>D. Hatziaframidis, “Stability of thin evaporating/condensing films in the presence of surfactants,” *Int. J. Multiphase Flow* **18**(4), 517–530 (1992).
- <sup>13</sup>D. Gallez, N. M. C. Pinto, and P. M. Bisch, “Nonlinear dynamics and rupture of lipid bilayers,” *J. Colloid Interface Sci.* **160**(1), 141–148 (1993).
- <sup>14</sup>T. Erneux and S. H. Davis, “Nonlinear rupture of free films,” *Phys. Fluids A* **5**(5), 1117–1122 (1993).
- <sup>15</sup>D. Vaynblat, J. R. Lister, and T. P. Witelski, “Rupture of thin viscous films by van der Waals forces: Evolution and self-similarity,” *Phys. Fluids* **13**(5), 1130–1140 (2001).
- <sup>16</sup>A. De Wit, D. Gallez, and C. I. Christov, “Nonlinear evolution equations for thin liquid films with insoluble surfactants,” *Phys. Fluids* **6**(10), 3256–3266 (1994).
- <sup>17</sup>J.-M. Chomaz, “The dynamics of a viscous soap film with soluble surfactant,” *J. Fluid Mech.* **442**, 387–409 (2001).
- <sup>18</sup>D. A. Edwards and A. Oron, “Instability of a non-wetting film with interfacial viscous stress,” *J. Fluid Mech.* **298**, 287–309 (1995).
- <sup>19</sup>R. J. Braun, S. A. Snow, and U. C. Pernisz, “Gravitational drainage of a tangentially-immobile thick film,” *J. Colloid Interface Sci.* **219**(2), 225–240 (1999).

- <sup>20</sup>O. K. Matar, “Nonlinear evolution of thin free viscous films in the presence of soluble surfactant,” *Phys. Fluids* **14**(12), 4216–4234 (2002).
- <sup>21</sup>E. Vignati, R. Piazza, and T. P. Lockhart, “Pickering emulsions: Interfacial tension, colloidal layer morphology, and trapped-particle motion,” *Langmuir* **19**(17), 6650–6656 (2003).
- <sup>22</sup>M. Mayarani, M. G. Basavaraj, and D. K. Satapathy, “Viscoelastic particle-laden interface inhibits coffee-ring formation,” *Langmuir* **34**(47), 14294–14301 (2018).
- <sup>23</sup>G. G. Fuller and J. Vermant, “Complex fluid-fluid interfaces: Rheology and structure,” *Annu. Rev. Chem. Biomol. Eng.* **3**, 519–543 (2012).
- <sup>24</sup>D. A. Edwards and D. T. Wasan, “A micromechanical model of linear surface rheological behavior,” *Chem. Eng. Sci.* **46**, 1247–1257 (1991).
- <sup>25</sup>D. E. Tambe and M. M. Sharma, “The effect of colloidal particles on fluid-fluid interfacial properties and emulsion stability,” *Adv. Colloid Interface Sci.* **52**, 1–63 (1994).
- <sup>26</sup>K. D. Danov, D. S. Valkovska, and I. B. Ivanov, “Effect of surfactants on the film drainage,” *J. Colloid Interface Sci.* **211**, 291–303 (1999).
- <sup>27</sup>L. Gary Leal, *Advanced Transport Phenomena* (Cambridge University Press, Cambridge, England, 2007), pp. 429–523.
- <sup>28</sup>S. S. Sadhal and R. E. Johnson, “Stokes flow past bubbles and drops partially coated with thin films. Part 1. Stagnant cap of surfactant film—exact solution,” *J. Fluid Mech.* **126**, 237–250 (1983).
- <sup>29</sup>J. M. Lopez and A. H. Hirs, “Surfactant-influenced gas-liquid interfaces: Non-linear equation of state and finite surface viscosities,” *J. Colloid Interface Sci.* **229**(2), 575–583 (2000).
- <sup>30</sup>J. C. Berg, *An Introduction to Interfaces & Colloids: The Bridge to Nanoscience* (World Scientific, 2010).
- <sup>31</sup>H. A. Stone, “A simple derivation of the time-dependent convective-diffusion equation for surfactant transport along a deforming interface,” *Phys. Fluids A* **2**(1), 111–112 (1990).
- <sup>32</sup>J. C. Slattery, L. Sagis, and E. Oh, *Interfacial Transport Phenomena* (Springer Science & Business Media, 2007).
- <sup>33</sup>H. Brenner, *Interfacial Transport Processes and Rheology* (Elsevier, 2013).
- <sup>34</sup>L. E. Scriven, “Dynamics of a fluid interface equation of motion for Newtonian surface fluids,” *Chem. Eng. Sci.* **12**, 98–108 (1960).
- <sup>35</sup>L. Ting, D. T. Wasan, K. Miyano, and S.-Q. Xu, “Longitudinal surface waves for the study of dynamic properties of surfactant systems. II. Air-solution interface,” *J. Colloid Interface Sci.* **102**, 248–259 (1984).
- <sup>36</sup>K. L. Maki and S. Kumar, “Fast evaporation of spreading droplets of colloidal suspensions,” *Langmuir* **27**, 11347–11363 (2011).
- <sup>37</sup>I. M. Krieger and T. J. Dougherty, “A mechanism for non-Newtonian flow in suspensions of rigid spheres,” *Trans. Soc. Rheol.* **3**, 137–152 (1959).
- <sup>38</sup>D. Quemada, “Rheology of concentrated disperse systems and minimum energy dissipation principle,” *Rheol. Acta* **16**, 82–94 (1977).
- <sup>39</sup>N. Alleborn and H. Raszillier, “Spreading and sorption of droplets on layered porous substrates,” *J. Colloid Interface Sci.* **280**, 449 (2004).
- <sup>40</sup>W. Kloek, T. van Vliet, and M. Meinders, “Effect of bulk and interfacial rheological properties on bubble dissolution,” *J. Colloid Interface Sci.* **237**, 158 (2001).
- <sup>41</sup>L. N. Trefethen, *Spectral Methods in MATLAB* (Oxford University, Oxford, England, 2000).
- <sup>42</sup>M. Dey, A. S. Vivek, H. N. Dixit, A. Richhariya, and J. J. Feng, “A model of tear-film breakup with continuous mucin concentration and viscosity profiles,” *J. Fluid Mech.* **858**, 352–376 (2019).
- <sup>43</sup>D. T. Wasan, A. D. Nikolov, L. A. Lobo, K. Kocz, and D. A. Edwards, “Foams, thin films and surface rheological properties,” *Prog. Surf. Sci.* **39**, 119–154 (1992).
- <sup>44</sup>D. Langevin, “Influence of interfacial rheology on foam and emulsion properties,” *Adv. Colloid Interface Sci.* **88**, 209–222 (2000).
- <sup>45</sup>B. S. Murray and R. Ettelaie, “Foam stability: Proteins and nanoparticles,” *Curr. Opin. Colloid Interface Sci.* **9**, 314–320 (2004).
- <sup>46</sup>P. Walstra, *Physical Chemistry of Foods* (Marcel Dekker, New York, 2003), p. 539.
- <sup>47</sup>A. Martin, K. Grolle, M. Bos, M. Stuart, and T. van Vliet, “Network forming properties of various proteins adsorbed at the air-water interface in relation to foam stability,” *J. Colloid Interface Sci.* **254**, 175–183 (2002).
- <sup>48</sup>P. Aussillous and D. Quéré, “Liquid marbles,” *Nature* **411**, 924–927 (2001).
- <sup>49</sup>L. Mahadevan, H. A. Stone, A. B. Subramaniam, and M. Abkarian, “Colloid science: Non-spherical bubbles,” *Nature* **438**, 930 (2005).
- <sup>50</sup>H. N. Dixit and G. M. Homsy, “The elastic Landau-Levich problem,” *J. Fluid Mech.* **732**, 5–28 (2013).
- <sup>51</sup>C.-C. Hwang, J.-L. Chen, and L.-F. Shen, “Nonlinear rupture theory of a thin free liquid film with insoluble surfactant,” *J. Phys. Soc. Jpn.* **65**(8), 2494–2501 (1996).